

Three-dimensional models of cloud evolution via ambipolar diffusion

Nikos Mastrodemos¹ and William D. Langer²

MS 169-506, Jet Propulsion Laboratory, California Institute of Technology, Pasadena, CA 91109

Richard Nelson, Astronomy Unit, School of Mathematical Sciences, Queen Mary & Westfield College, Mile End Road, London E1 4NS

ABSTRACT

We present three-dimensional smoothed particle hydrodynamics models for the evolution of magnetically supported clouds by ambipolar diffusion. Our models include detailed heating and cooling mechanisms, radiation by the external UV field, and a gas-phase chemical network. The magnetic field is approximated by a scalar field which supports the spherical cloud through magnetic pressure. Similarly ambipolar diffusion is modeled by a scalar diffusion equation. We examine the ambipolar diffusion timescale and the formation of magnetically supercritical cores as a function of the interstellar UV flux, central cloud density, initial metal abundance and cosmic-rate ionization rate. The evolutionary timescale depends sensitively on the central density of the clouds, with dense clouds, $n = 2 \times 10^3 \text{ cm}^{-3}$ evolving by at least an order of magnitude faster than lower density clouds, $n = 400 - 750 \text{ cm}^{-3}$. The low density clouds, maintain a relatively high fractional ion abundance in their cores requiring a time of 10^8 years to reach higher central densities. These clouds probably will not be observed forming dense cores. In all models studied we found that the interstellar UV field essentially controls the rate of field diffusion at the cloud core with an increase in the UV resulting in an increase in the field diffusion timescale. An increase in the initial metal abundance also increases substantially the diffusion timescale. As in past works we confirm that ambipolar diffusion leads to low efficiency star formation with the collapsing supercritical cores having masses in the range, $4.5 - 6 M_{\odot}$ and radii $0.12 - 0.17 \text{ pc}$.

1. Introduction

The formation of dense cloud cores within molecular clouds is an important phase in theories of star formation, involving many complex physical processes that are not yet fully understood. Such cores have typical sizes of $\simeq 0.1 \text{ pc}$, temperatures $\approx 10 \text{ K}$, and average densities $\simeq 10^4 \text{ cm}^{-3}$.

¹mastro@thisvi.jpl.nasa.gov

²langer@nimba.jpl.nasa.gov

Observations of the physical properties and magnetic fields in molecular clouds (e.g., Myers and Goodman 1988a, 1988b; Goodman et al. 1989; Roberts et al. 1993; Crutcher et al. 1993; Güsten Fiebig and Uchida 1994; Crutcher et al. 1996; Troland et al. 1996; Crutcher et al. 1999), suggest that magnetic fields are at least essential and often the dominant ingredients for the stability of clouds against gravitational collapse. The stability conditions of magnetized clouds have been established in detail (Strittmatter 1966; Mouschovias 1976; Mouschovias and Spitzer 1976; Langer 1978; Tomisaka, Ikeuchi and Nakamura 1988). An important process by which dense cores and stars form within magnetically subcritical molecular clouds is ambipolar diffusion, the relative drift of neutrals through ions in a partially ionized medium (Mestel and Spitzer 1956). Analytical work and a large number of numerical calculations in the past 20 years have treated many aspects of the problem and elucidated in detail the essentials of the mechanism and the relevant physical processes on various levels of approximations and geometries (e.g., Tomisaka, Ikeuchi and Nakamura 1990; Mouschovias 1979, 1991; Lizano and Shu 1989; Nakano 1979, 1983; Fiedler and Mouschovias 1993; Ciolek and Mouschovias 1993, 1994, 1995 (hereafter CM94, CM95); Basu and Mouschovias 1994, 1995, and references therein).

The latest summary and interpretation of measurements of magnetic field strengths in molecular clouds (Crutcher 1999 and references therein) indicate that although magnetic fields are dynamically important, a complete picture of star formation should include other essential physical mechanisms, notably turbulent gas motions. These works suggest that it is important to consider ambipolar diffusion in conjunction with other physical processes, such as turbulence, outflows, external shocks with the aim of building more comprehensive models of cloud fragmentation and collapse. As a step in this direction here we extend previous smoothed particle hydrodynamic (SPH) modeling efforts (Nelson and Langer 1997; Nelson and Langer 1999) to include in an approximate way the effects of magnetic fields and ambipolar diffusion in three-dimensions, while treating the cloud from a global perspective, considering the coupled dynamical, thermal, chemical and radiative problem. Our main focus is the quiescent evolution of clouds that are in a pre-collapse, gravitationally bound state, i.e., densities in the $10^2 - 10^3 \text{ cm}^{-3}$ range, under the assumption that magnetic fields are essential for the gravitational support of the cloud.

In this first work we describe our modeling method and we obtain simple solutions of spherical clouds as a first step towards exploring fragmentation in more complex geometries. Our objective is to validate our method by producing physically meaningful results and study cloud evolution and core formation as a function of central density, n_c , external UV field, cosmic-rate flux and initial metal abundance.

The paper is organized as follows. In section 2 we summarize the physics of the models and our approximate description of magnetic fields, in section 3 the numerical method, in section 4 we discuss our results, in section 5 we compare with previous modeling efforts and in section 6 we summarize our conclusions.

2. The physics of the cloud models

The details of the physical ingredients included in the cloud models have been described in detail in Nelson & Langer (1997, 1999, hereafter NL97, NL99) where we refer the reader for a complete discussion. Here we describe the extensions to our current models.

2.1. Thermal model

Cooling includes molecular line cooling through an analytical fit based on the calculations of Goldsmith & Langer (1978), appropriate for $T < 100$ K, and fine-structure cooling of O I, C I and C II. To improve line cooling for $T > 100$ K, which can occur at the low density outer parts of the clouds, we have modified the Goldsmith & Langer cooling to include rotational transitions of CO and H₂O following the four parameter fit to the cooling function from Neufeld & Kaufman (1993), Neufeld, Lepp & Melnick (1995). Heating sources include the cosmic-ray ionization, H₂ formation on grains and the photoelectric ejection of electrons from grains, which is caused by the interstellar radiation field. The total UV extinction to any location within a cloud is computed by an approximate ray-tracing calculation, whereby the optical depth at a certain location in the cloud is approximated as the average of six optical depths along the positive and negative direction of the three coordinates. The thermal energy exchange between grains and gas is also a heating/cooling source depending on the temperature difference between the grains and the gas.

2.2. Chemical model

Following the chemistry in the gas with the dynamical evolution is important for determining the abundance of the various molecular tracers and coolants. For magnetically supported clouds it is of particular importance for the accurate determination of the total ionic abundance and hence the strength of coupling between magnetic fields and neutrals.

The chemical model is the same as described in NL99 with some modifications and extensions in order to improve the determination of the ion abundance. The cloud consists of H₂ and traces of molecules. We describe explicitly the chemical evolution of the species: He⁺, H₃⁺, OH_x, CH_x, CO, C, C⁺, HCO⁺, O, M, M⁺ and e⁻. OH_x is a composite of O₂, H₂O and OH, CH_x of CH₂ and CH, and M collectively describes the metals, Fe, Si, Mg, Ca, Na, in order to simplify the total number of equations.

The modifications in the reaction rates of the chemical network used in NL99 are as follows: The $C^+ + H_2 \rightarrow CH_x + H$ reaction rate is made temperature dependent, $4 \cdot 10^{-16} (T/300)^{-0.2} \text{ cm}^3 \text{ s}^{-1}$. The ionic metal removal rate, $M^+ + e^- \rightarrow M + h\nu$ is modified to be $1.5 \cdot 10^{-10} T^{-0.6} \text{ cm}^3 \text{ s}^{-1}$. This rate is adopted from the corresponding Si^+ rate of the UMIST database (Millar et al. 1995). Here we assume that the larger initial ionic metal contribution comes from Si^+ and Fe^+ with the

number ratio $Si/Fe = 5$ and the initial condition $n(M_{total}) = n(M^+)$. The recombination rate of H_3^+ is $1.5 \cdot 10^{-7} (T/300)^{-0.5} \text{ cm}^3 \text{ s}^{-1}$, following the more recent results from Sundstrom et al. (1993).

In addition to the photoreactions caused by the external UV field we now include the effects of the UV field which is locally induced by the cosmic ray excitation cascade. This is accomplished by considering the same reactions and adding to the rates of the external UV field the rates of the cosmic ray induced field which are written as, $k = \zeta_p(H_2)\gamma_{cr}/(1 - \omega) \text{ s}^{-1}$, (Millar et al. 1995). Here k is the cosmic ray induced photorate, $\zeta_p(H_2)$ the primary cosmic-ray ionization rate, γ_{cr} the probability per cosmic-ray ionization that the respective photoreaction occurs, and ω is the grain albedo in the far UV. Values of γ_{cr} were taken from Millar et al. (1995) and for all models we assume $\omega = 0.5$. For the C^+ and M^+ producing photoreactions the cosmic-ray induced ionization begin to dominate over the external radiation at visual optical depths of 1.5 and 1.4 respectively. For intermediate core densities during cloud evolution, $10^3 \leq n(H_2) \leq 10^6 \text{ cm}^{-3}$, cosmic-ray induced photo-ionization is the dominant factor for the ionization of metals.

To test the accuracy of our simplified chemistry to reproduce correctly the electron abundance as a function of density and temperature in the cloud interior, we compare it to gas-phase subset of the UMIST RATE95 stand-alone chemical network (Millar et al. 1995) which includes a total of 82 reactions (fig. 1) but does not include grain chemistry. The data from the hydrodynamic calculations at the lower densities were drawn from the centers of more than one cloud model, although most were from model M3 (see below). Overall there is good agreement between the total e^- of the two chemical networks. The largest differences occur at the lower densities. Below $n(H_2) \simeq 4 \times 10^3 \text{ cm}^{-3}$ our code underestimates the total e^- abundance by at most a factor of two, but at $n(H_2) \geq 5 \times 10^3$ agreement becomes very good, with a fractional difference for most data points of $< 5\%$. Furthermore as ambipolar diffusion becomes important at higher densities our simplified model of electron and ion abundance is well suited to the model calculations.

2.3. Magnetic fields and ambipolar diffusion

MHD calculations with field diffusion have been performed in 2-D axisymmetric geometries (Fiedler and Mouschovias 1993) (other refs), plane-parallel (Nakano, Fiedler others) and 1-D (Ciolek and Mouschovias 1994; Ciolek and Mouschovias 1995) as well as in 3-D. 3-D axisymmetric cloud collapse calculations with field diffusion were performed by Nakano Lizano and Shu (1989), Tomisaka, Ikeuchi and Nakamura (1990) and Boss (1997). Most three-dimensional models follow the quasi-static cloud evolution. Boss (1997) made the simplification of a scalar field which contributes to cloud support through the magnetic pressure term, while ignoring magnetic tension. However field diffusion in Boss (1997) was treated as removal of the magnetic flux from the whole cloud rather than flux redistribution within the cloud.

These model calculations have as initial conditions simple field geometries, with straight field

lines of large-scale ordered fields. These geometries inevitably lead to the formation of flattened disks. In fact the calculations of CM94, CM95 are essentially one-dimensional models of a disk with azimuthal symmetry. Other analytical works at various degrees of approximation tackled the quasi-static pre-collapse phase as well as the later stages of core evolution under the assumptions of spherical or disk-like geometries (Safier, McKee and Stahler 1997; Li and Shu 1997; Li 1998; Li 1998; Contopoulos, Ciolek and Königl 1998). Most of these calculations make the assumption that clouds are isothermal or neglect thermal pressure.

Existing numerical calculations although treating the full MHD problem begin with the assumptions of ordered fields. On the other hand observations suggest that clouds are close to magnetic and virial equilibrium (e.g., Myers and Goodman 1988a, Crutcher 1999) and simulations of decaying and driven turbulence show that initially straight field lines can become distorted (Mac Low 1999; Ostriker, Gammie and Stone 1999). Observations also indicate that clouds, including their dense cores, do not evolve to become two-dimensional pancakes, but rather prolate spheroids (Myers et al. 1991; Ryden 1996), suggesting that thermal, turbulent or magnetic forces contribute to their support. The assumption of disordered fields on short scales may be reasonable for a significant subset of interstellar clouds.

As a first approximation to a full MHD description in 3-D, in order to keep calculations manageable, we employ a restricted version of the equations, which still captures many of the essentials of cloud collapse under the combined effects of ambipolar diffusion and cooling. In our description the magnetic field is considered “tangled-up” and approximated by a scalar field which contributes to cloud support through its magnetic pressure (Boss 1997, Safier et al. 1997, Li 1998). Clouds are considered spherical which again is an approximation of the more general prolate shapes (Myers et al. 1991, Ryden 1996) in order to be consistent with the isotropic magnetic pressure assumption. For comparisons with observations the validity of our conclusions should scale with the degree of elongation of actual clouds.

More specifically, in the low ionization regime of interest the inertia and pressure forces of the ions can be neglected compared to that of the neutrals. The momentum equation for the neutrals reduces to equating the magnetic and drag forces,

$$\gamma_i \rho_i \rho_n (\mathbf{v}_i - \mathbf{v}_n) = \frac{1}{4\pi} (\nabla \times \mathbf{B}) \times \mathbf{B} = -\nabla \left(\frac{\mathbf{B}^2}{8\pi} \right) + \frac{1}{4\pi} (\mathbf{B} \cdot \nabla) \mathbf{B} \quad (1)$$

where ρ_i , ρ_n , \mathbf{v}_i , \mathbf{v}_n are the ion and neutral mass densities and velocities and γ_i is the collisional coupling term between ionic species i and neutrals,

$$\gamma_i = \frac{\langle \sigma w \rangle_{in}}{m_i + m_n} \quad (2)$$

and $\langle \sigma w \rangle_{in}$ is the average collisional rate between ions and neutrals, m_i the mass of the ion and

$m_n = m_{H_2}$ the mass of the neutral. By solving in equation (1) for the ion velocity and substituting in the induction equation,

$$\frac{\partial \mathbf{B}}{\partial t} = \nabla \times (\mathbf{v}_i \times \mathbf{B}) \quad (3)$$

we have in Lagrangian coordinates the evolution of the magnetic field as,

$$\frac{d\mathbf{B}}{dt} = (\mathbf{B} \cdot \nabla) \mathbf{v} - \mathbf{B}(\nabla \cdot \mathbf{v}) + \frac{1}{4\pi\gamma_i\rho_i\rho_n} \nabla \times \{[(\nabla \times \mathbf{B}) \times \mathbf{B}] \times \mathbf{B}\} \quad (4)$$

Hereafter \mathbf{v} refers to the velocity of the neutrals and the ions do not appear explicitly in the dynamical equations. The first term in the above expression represents the field evolution from the velocity shear, the second term from the compression or expansion of the fluid, and the third term ambipolar diffusion. Our simplifying assumptions for a scalar field amount to dropping the magnetic tension term from equation (1) and the shear term from equation (4). In order to conserve magnetic flux, the second term in equation (4), which now describes the frozen-in field evolution must be modified to read, $-\frac{2}{3}B(\nabla \cdot \mathbf{v})$. Note that by making use of the continuity equation,

$$\frac{d\rho}{dt} = -\rho \nabla \cdot \mathbf{v} \quad (5)$$

this relation reduces to $B = B_o (\rho/\rho_o)^{2/3}$, which is what we use for the frozen-in field evolution. We finally replace the ambipolar diffusion term with a diffusion equation for a scalar field, so that equation (4) becomes,

$$\frac{dB}{dt} = -\frac{2}{3} B(\nabla \cdot \mathbf{v}) + \frac{1}{4\pi\gamma_i\rho_i\rho_n} \nabla \cdot (B^2 \nabla B) \quad (6)$$

The final form of the momentum equation reads,

$$\frac{d\mathbf{v}}{dt} = -\frac{1}{\rho} \nabla \left(P + \frac{B^2}{8\pi} \right) - \nabla \Phi \quad (7)$$

where Φ is the gravitational potential. For completeness the energy equation is written as

$$\frac{dU}{dt} = -\frac{P}{\rho} \nabla \cdot \mathbf{v} + \frac{\Gamma - \Lambda}{\rho} \quad (8)$$

with Γ and Λ the nonadiabatic heating and cooling sources. The fluid equations are closed with an equation of state,

$$P = \frac{\Re}{\mu} \rho T = K(S) \rho^\gamma \quad (9)$$

where \Re is the gas constants, μ the mean molecular weight, T the temperature, $K(S)$ a function of the entropy and γ the ratio of specific heats which is taken to be 5/3. The chemical rate equations are written as,

$$\frac{dX_i}{dt} = nK_i \quad (10)$$

where X_i is the fractional abundance of species i , K_i the corresponding reaction rate and n the gas number density.

3. Numerical methods

The fluid and chemical equations are solved using a smoothed particle hydrodynamics method (Lucy 1977, Gingold & Monaghan 1977). The version of SPH we employ uses a variable smoothing length (Hernquist & Katz 1989) in the conservative formulation of Nelson & Papaloizou (1994). The gravitational potential is solved with a treecode (Hernquist & Katz 1989). Details of the particular SPH formulation along with test problems are presented in Nelson & Papaloizou (1994). For the results presented here the number of SPH particles was $N = 40,000$, for the low density clouds with an expected long evolutionary timescale, and $N = 50,000$ for the rest. The chemical network, comprises a system of ten stiff ordinary differential equations, which is solved implicitly for each SPH particle and at each timestep using the LSODE routine. The solution of the chemical equations for the whole cloud comprises $\sim 55\%$ of the total cpu time per cycle and is the major limitation for considering a larger number of particles or chemical reactions.

3.1. Magnetic field evolution

The flux-freezing part of the field evolution is numerically performed as

$$B^{n+1} = B^n \left(\frac{\rho^{n+1}}{\rho^n} \right)^{2/3} \quad (11)$$

where the superscript denotes time levels. The diffusion term is more conveniently written as,

$$\left(\frac{dB}{dt} \right)_{diff} = \frac{1}{4\pi \langle \gamma f \rangle} \nabla \cdot \left(\frac{B^2}{\rho^2} \nabla B \right) \quad (12)$$

where $f_i = \frac{\rho_i}{\rho} = X_i \frac{m_i}{m_{H_2}}$ and

$$\langle \gamma f \rangle = \sum_{i=1}^5 \gamma_i f_i = \sum_{i=1}^5 X_i \frac{m_i}{m_{H_2}} \frac{\langle \sigma w \rangle_{in}}{m_i + m_{H_2}} \quad (13)$$

for the 5 ionic species, C^+ , M^+ , H_3^+ , He^+ and HCO^+ . Note that the gas density remains unchanged during the field time integration. To avoid taking second derivatives of the spline kernel, for the SPH formalism of expression (12) we adopt the method first described by Brookshaw (1985), see also Monaghan (1992). For a one-dimensional diffusion equation, $\frac{d}{dx}(\eta \frac{dT}{dx})$ this method consists of taking the first derivative of the kernel and a finite difference of the diffused variable T , so that the SPH equivalent becomes,

$$\frac{d}{dx} \left(\eta \frac{dT}{dx} \right)_i = \sum_j \frac{m_j}{\rho_j} \frac{(Q_i + Q_j)(T_i - T_j)}{(x_i - x_j)} \frac{\partial W_{ij}}{\partial x_i} \quad (14)$$

where the summation extends over the nearest neighbors of particle i . The generalization of this prescription in 3 dimensions for expression (12) is

$$\left(\frac{dB}{dt} \right)_{diff}^i = \frac{1}{4\pi} \sum_j \frac{m_j}{\bar{\rho}_{ij}} \frac{(\frac{B_i^2}{\rho_i^2} + \frac{B_j^2}{\rho_j^2})(B_i - B_j)}{\langle \gamma f \rangle_{ij} (|\mathbf{r}_{ij}|^2 + \epsilon \bar{h}_{ij}^2)} \mathbf{r}_{ij} \cdot \frac{1}{2} [\nabla_i W(\mathbf{r}_{ij}, h_i) + \nabla_j W(\mathbf{r}_{ij}, h_j)] \quad (15)$$

for the symmetrized kernel formalism we employ. Here $\bar{\rho}_{ij} = (\rho_i + \rho_j)/2$, $\overline{\langle \gamma f \rangle}_{ij} = (\langle \gamma f \rangle_i + \langle \gamma f \rangle_j)/2$, $\bar{h}_{ij} = (h_i + h_j)/2$, $\mathbf{r}_{ij} = \mathbf{r}_i - \mathbf{r}_j$, and h is the smoothing length. The term $\epsilon \bar{h}_{ij}^2$ is added to prevent numerical divergences, and $\epsilon = 0.01$. This expression is symmetric with respect to particles i and j so that exchange of flux between i and j conserves their total flux, $(dB/dt)_{ij} = -(dB/dt)_{ji}$, and the total flux is conserved since $\sum_{i=1}^N (\frac{dB}{dt})_{diff}^i = 0$. Our tests, including the models we present here, have shown that the above form of the diffusion equation conserves the total flux to a satisfactory degree. The relative error at each timestep, dt , $dt \sum_{i=1}^N (\frac{dB}{dt})_{diff}^i / \sum_{i=1}^N B_i$ fluctuates between $\pm 10^{-10}$ with an average value $\sim 10^{-11}$ and with no trend for any systematic build-up during time integration over many thousands of timesteps. When the characteristic diffusion timestep, $dt_{diff} = \frac{4\pi \langle \gamma f \rangle \rho h^2}{B^2}$ is smaller than the dynamical timestep the diffusion part is performed iteratively within each dynamical step, although for the models examined here the dynamical timestep was a factor of a few smaller than the diffusion one.

For these first series of calculations we adopted a single value for the ion-neutral average collisional rate for all ions, $\langle \sigma w \rangle_{in} = 1.7 \cdot 10^{-9} \text{ cm}^3 \text{ s}^{-1}$ which is very close to the $\text{HCO}^+ - \text{H}_2$ collisional rate (Paleologou and Mouschovias 1983).

3.2. Parameter space

Modeling of cloud evolution via ambipolar diffusion in three dimensions is a particularly cpu-intensive computation and a full parameter space exploration is beyond the scope of the present work. Instead we chose to highlight a few specific questions with a moderate number of models. Parameters that we varied in our models are 1) the initial total metal abundance 2) the cosmic-ray ionization rate, 3) the initial central density and magnetic field and 4) the extinction that the interstellar radiation field suffers before it reaches the cloud's outer boundary.

We examine spherical clouds with mass $400 M_\odot$. Clouds are centrally condensed and initial central densities vary, with $n_c = 400 \text{ cm}^{-3}$ for the low density clouds to $n_c \simeq 2 \times 10^3 \text{ cm}^{-3}$. The stability criterion, in a formal sense, of the clouds is determined as follows. Starting from

an equation of motion which includes only the magnetic pressure term and not the magnetic tension term, e.g., Chandrasekhar (1961), assuming initially static clouds and neglecting the external pressure we derive the stability condition, $2E_{th} + 3E_m > E_g$, where E_m and E_{th} are the total magnetic and thermal energies respectively and E_g is the absolute value of the potential gravitational energy. The additional contribution of $2E_m$ comes from the lack of the magnetic tension term which appears in the form $-2E_m$ in the Virial theorem. The magnetic stability criterion is $3E_m > E_g$ and we refer to clouds that satisfy it as being magnetically subcritical and clouds or portions thereof with $3E_m < E_g$ as supercritical. For the models we present in this work we performed stability tests in the absence of thermal pressure and field diffusion and found that they are stable when $E_m/E_g \geq 0.36 - 0.38$, which is reasonably close to the formal limit of 0.33, given that this limit does not include the effects of the external pressure. During cloud evolution we use the criterion $\gamma \equiv (2E_{th} + 3E_m)/E_g$ to establish the portions of the clouds which become unstable, $\gamma < 1$. In general, because of thermal pressure cloud portions become first supercritical and then unstable. We also define $\alpha = E_{th}/E_g$ and $\beta = E_m/E_g$, and we use the criteria, $2\alpha < 1$ and $3\beta < 1$ to determine the cloud portions which become thermally unstable or supercritical respectively.

Most clouds are magnetically subcritical, except M2 which is marginally supercritical but globally stable. For low density clouds the balance of heating and cooling sources establishes an initial temperature profile which allows the clouds to be initially thermally stable, although marginally so in models M1 and M2. Without an additional means of support, cooling would eventually render these clouds thermally unstable (e.g., Nelson and Langer 1997). The inclusion of magnetic support may allow such clouds to remain stable indefinitely even though they are marginally supercritical, and M2 is such an example.

The primary cosmic ray ionization rate, and the initial fractional metal abundance, were treated as free parameters in the range $\zeta_p(H_2) = 1 - 5 \times 10^{-17} \text{ s}^{-1}$, and $[M]/[n(H_2)] = 10^{-8} - 10^{-7}$ respectively to reflect uncertainties in their observationally determined values (e.g., Williams et al. 1998; Bergin et al. 1999). In order to reduce run-time all models except one are run with the combination of values that would allow for the shorter field diffusion timescale, i.e., $\zeta_p(H_2) = 10^{-17} \text{ s}^{-1}$ and $[M]/[n(H_2)] = 10^{-8}$. We produced one model with the combination $\zeta_p(H_2) = 5 \times 10^{-17} \text{ s}^{-1}$ and $[M]/[n(H_2)] = 10^{-7}$ to test the increase of the ambipolar diffusion timescale, t_{ad} , as a function of these parameters.

Variation in the interstellar radiation field is included in order to examine how the external cloud environment can affect its evolution. Here we have chosen two different values: 1) The standard interstellar UV flux ($G_o = 1$) and 2) a value equal to 0.16 of the standard value, which corresponds to two magnitudes of UV extinction at the outer cloud boundary. The standard UV flux represents evolution of a cloud in isolation whereas the reduced value can be thought of as representing evolution of a cloud or sub-condensation which resides in the interior of a larger cloud complex, so that significant attenuation of the ambient UV flux has taken place. In all models the UV field is isotropic.

In Table 1 we summarize most of the important initial parameters of the models; cloud mass and radius, initial central number density, initial central magnetic field, the stability criterion, γ , the initial ratio of magnetic and thermal to gravitational energy and the factor by which the UV field differs from the standard interstellar value. Table 2 contains the ambipolar diffusion time for each model and the collapsed core mass and radius at the end of the calculation.

3.3. Set-up of initial and boundary conditions

Initial distribution of particles is with a rejection/acceptance method, set to mimic a $\rho \sim r^{-1}$ density profile with the superposition of a Gaussian profile for the inner cloud. Such a configuration allows for rapid relaxation to a quasi-static equilibrium where the cloud executes small radial oscillations with a small radial velocity amplitude, $|v_r| < 0.2c_s$ where c_s is the isothermal speed of sound, and with average $v_r \simeq 0$. For computational purposes, a centrally condensed configuration was found preferable to a uniform one as it allows a faster relaxation to a quasi-static equilibrium and also a smaller exterior boundary pressure (see below).

The initial velocity is set to zero in all models presented here. As confirmed by NL99 when a spectrum of turbulent velocity fluctuations is initially imposed on the cloud, dissipation of turbulence on small scales occurs within a fraction of the sound crossing time. The subsequent evolution is very similar to that of a cloud with zero initial velocity. Tests we conducted for magnetized clouds exhibited the same behavior; a rapid dissipation within a fast magnetosonic crossing time, and subsequent evolution to a centrally condensed cloud which evolves quasi-statically under field diffusion. No evidence of cloud fragmentation was produced by applying an initial spectrum of velocity fluctuations.

After the density profile is determined, the initial magnetic field is determined by choosing its central value and making use of the relation $B \sim \rho^{2/3}$. All cloud models presented here were run for many (> 10) free-fall times with ambipolar diffusion turned off in order to establish their stability and average density profile. In the absence of field diffusion, after a rapid relaxation phase, the clouds remain in a quasi-static stable configuration, undergoing small amplitude radial oscillations. The central magnetic field is set to the value that will allow the desired time-averaged value for the central density. Any evolution towards greater central densities is solely the result of ambipolar diffusion.

The gravitational softening radius was chosen to be 10^{-4} of the cloud radius, after extensive testing with the current models (as well as in NL99). That particular value is determined by the requirement of sufficient numerical resolution of the innermost cloud core, for a given total number of SPH particles. For the clouds which form dense cores their evolution is followed until the peak number density reaches $n(H_2) = 10^{11} - 10^{12} \text{ cm}^{-3}$, which represents an increase in density of more than eight orders of magnitude from the initial central density values.

Appropriate boundary conditions are those that simulate in an approximate manner the

confining environment of the cloud. Here we consider two cloud categories; isolated ones, ($G_o = 1$) and embedded ones, that are thought-of as condensations within a larger cloud ($G_o = 0.16$). In both cases magnetized model clouds need to be confined by an external pressure, P_{ext} , to prevent them from freely expanding into a vacuum. In addition when $G_o = 1$ the outer layers of the cloud can be heated to $T > 100$ K and photoevaporate (see for example NL97). In principle expansion of the outer cloud layers can also take place as a result of diffusion of magnetic flux from the cloud interior. The initial density of the cloud models at their outer boundary is in the range 30 - 300 cm^{-3} , depending on the model, with the lower central density clouds having the lower boundary densities. We estimate P_{ext} by making the assumption that the diffuse medium surrounding the cloud has density comparable to that of the outer cloud layers and that the magnetic field in the diffuse medium follows the same $B - \rho$ scaling as in the cloud interior. We set P_{ext} equal to the combined magnetic and thermal pressure of the cloud boundary. The implementation of this boundary condition in the momentum equation is described in NL99. This matching is not exact during cloud evolution since field diffusion and heating can cause cloud expansion. In practice the clouds undergo a slow expansion which amounts to an increase of a few percent of the original cloud radius. This boundary condition is not meant to represent an accurate description of the cloud boundary interface but rather a compromise between a physically reasonable external pressure and the practical issue of confining the cloud for a time interval comparable to the field diffusion timescale. The outer boundary condition is supplemented by a zero ambipolar diffusion rate across the cloud boundary. This choice is justified by the fact that the ionization fraction at the outer cloud layers and the corresponding diffusion timescale are a few orders of magnitude higher than in the cloud interior so that practically no magnetic flux leaves the cloud.

All models were constructed with the same initial chemical fractional abundances, with the exception of one model (M5) with a higher initial metal abundance. These are: $n(C_{total}) = 10^{-4} n(H_2)$, $n(O_{total}) = 2 \times 10^{-4} n(H_2)$, $n(He_{total}) = 0.28 n(H_2)$, with $n(CI) = n(CO) = n(CH_x) = n(HCO^+) = 0$, $n(C^+) = n(C_{total})$, $n(OI) = n(O_{total})$, and $n(M^+) = n(M_{total})$.

4. Results

4.1. A typical example of collapse

In this section we describe the evolution of a cloud model, M3, with $M = 400M_\odot$, $n_c \simeq 2 \times 10^3$ cm^{-3} , as a representative example of a collapsing cloud. The main features of the evolution of the other collapsing models are qualitatively similar. This particular model has the lowest value of α , so that thermal effects have a smaller influence in its evolution compared to the other models (see Table 1).

In figures 2, 3, 4 and 5 we display the time evolution of the model. In figure 2 we display the radial profiles of the number density of molecular hydrogen, the magnetic field and the gas

temperature, the radial component of the gas velocity, with negative values indicating inflow and positive values outflow and the magnetic field diffused at that particular timestep, with negative values indicating loss and positive values indicating gain of magnetic field through ambipolar diffusion.

In figure 3 we display at the same time as in figure 2 the radial profiles of the fractional abundances of the ten species of the chemical network as well as the e^- fractional abundance; the left panel includes the neutral species and the right panel the ions. During cloud evolution we monitor the total gravitational, thermal and magnetic energy of the whole cloud as well as portions of the cloud which are spherical volumes surrounding the origin at various radii. The gravitational potential energy for these spherical volumes is computed by direct summation for the particles interior to the particular volume. In figure 4 we display the time evolution of the thermal, 2α , magnetic, 3β and total, $\gamma = 2\alpha + 3\beta$, stability criteria for the whole cloud (4a) as well as for the volumes at radii, $r = 0.025$ and 0.1 pc (4b). At later stages of the evolution the innermost, $r = 0.025$ pc volume is a good representation of the average properties of the core cloud. In figure 5 we display the time evolution of the peak cloud density.

Figs. 2a, 3a show the state of the cloud at the beginning of its evolution, after one dynamical timestep, which is sufficient time to establish thermal equilibrium in the cloud. At this time the visual optical depth to the cloud center is $\simeq 2$ magnitudes and the ratio of magnetic to thermal pressure at the cloud center is 18. For the assumed UV extinction at the cloud boundary, $G_o = 0.16$, and cosmic-ray flux, the UV ionization rate of C equals the cosmic-ray ionization rate at $\tau_v \simeq 5$, and that of M at $\tau_v \simeq 8$, whereas for $G_o = 1$ this happens for values of τ_v higher by only a few decimal points. These values of τ_v are in general agreement with the extinction values for which cosmic-ray ionization exceeds UV ionization derived by McKee (1989). At the beginning of the evolution, therefore, the external UV field is the dominant ionizing agent; this is also the case for the initial state of all models studied. The temperature at the center has already attained the equilibrium value of gas at $n(H_2) \simeq 2 \times 10^3 \text{ cm}^{-3}$, which cools mostly by C^+ and CO emission, (fine-structure cooling of $C\text{ I}$, $O\text{ I}$ are not important at these densities) and is heated mainly by the external UV field. Because of the attenuation of the ambient UV radiation at the cloud boundary the temperature there is not much higher than at the center. Chemical differentiation has already started taking place in the cloud with large amounts of CO and $C\text{ I}$ produced in the interior. At the outer boundary, however, most of the carbon remains in C^+ , which is the dominant ionic contributor throughout the cloud.

After 2.24 free-fall times, figs. 2b, 3b, the central density has risen by a factor of 3. The density profile at $r > 0.5$ pc is very similar to the initial state and rises slowly inward of 0.5 pc. The cloud is overall stable with the evolution of its inner regions being the result of ambipolar diffusion, as can be seen by the loss of magnetic flux from the inner 0.2 pc. The radial velocity shows an oscillatory behavior about the cloud's static equilibrium and remains always subsonic (and sub-alfvenic) with $|v_r| < 0.3 \times c_s$. The cloud is in a quasi-static equilibrium and remains in that phase for most of its evolution. At this time the visual extinction to the cloud center is \simeq

5, with $\tau_v = 4$ at $r = 0.1$ pc, so that cosmic ray ionization starts becoming comparable to the ambient UV at the cloud core.

By that time significant chemical evolution has taken place in the cloud interior. The increased extinction has led to the conversion of C^+ into CO, with $X(C^+) = 2.3 \times 10^{-8}$ at the core. Most of C^+ is converted into CO and CI in a small transition zone around $r = 1$ pc. Here we can already see some differences in the profiles of the carbon species between magnetically and thermally supported clouds. Compared to the results of NL99 (fig. 2) the drop in the C^+ abundance is not as sharp. The primary reason is that the envelope is well supported which results in a shallower density profile. A contributing factor also is the adopted boundary condition which allows minimal cloud expansion. Another distinguishing feature, compared to NL99, is a secondary peak in the C I around $r = 0.25$ pc and an overall higher C I abundance interior to that location. Not shown at that scale the second C I peak corresponds to a depression in the CO profile at that radius, indicative of conversion of CO into C I. We attribute this both to the density profile established from magnetic support and to the inclusion of the cosmic-ray induced UV field. A similar cloud model which is only thermally supported has a steeper density profile and does not exhibit this secondary C I peak, although in general it maintains a higher C I abundance in the inner core than the NL99 models.

The stability of the cloud can be examined in fig. 4. As expected for a B - ρ power-law relation with $2/3$ exponent E_m/E_g for the whole cloud (4a) remains practically constant throughout the cloud's evolution and the same is true for E_{th}/E_g . In addition to their ratios E_m , E_g and E_{th} remain close to being constant during evolution, a result which indicates that contraction, and to a lesser degree cooling, of the inner cloud portions is balanced by a tendency for expansion as a result of the magnetic pressure and heating of the outer cloud envelope. In fig. 4b the central cloud volumes of 0.1 and 0.025 pc, remain stable for most of the evolution and the support is mainly due to the magnetic pressure. The gradual decrease of 2α with time is due to the slow increase in the density of the central regions, since the temperature variation is small there during evolution. The decrease of 3β is faster because of the attendant loss of magnetic flux in addition to the density increase. In the 0.1 pc volume the magnetic energy always remains higher than the thermal energy, however at $r < 0.025$ pc field diffusion allows the magnetic energy to become smaller than the thermal energy at $t > 4t_{ff}$, when the central density exceeds $4 \times 10^4 \text{ cm}^{-3}$. For the 0.05 pc volume, $E_m < E_{th}$ occurs for $t > 5t_{ff}$, or $n_c \geq 1.2 \times 10^5 \text{ cm}^{-3}$.

The continuous loss of magnetic flux from the inner core and its redistribution in the outer envelope allows the central density to increase while the cloud remains in quasi-static equilibrium (figs. 2c, 3c). Compared to the density profile the magnetic field remains much flatter in the inner 0.1 pc. The central magnetic field value is 38μ Gauss whereas a frozen-in field at that central density would have a value of 190μ Gauss. The radial velocity of the outer envelope, $r > 0.1 - 0.2$ pc, remains oscillatory with a time-averaged value over a few free-fall times at every radius approximately zero, whereas the inner envelope, $r < 0.1 - 0.2$ pc, shows a trend for an inward radial velocity which is $\leq 0.08 \times c_s$. At that time, $t = 3.86 t_{ff}$, at the cloud core $\tau_v = 8$ so

that the external UV radiation is unimportant in the chemical evolution of the cloud core. At the increased density of the central regions, the gas-dust thermal coupling starts becoming significant. Since the grains are maintained at their equilibrium 10 K temperature, they are a heating source for the gas, raising the temperature of the central regions towards 10 K. Between 0.1 and 0.6 pc however the cloud still remains cooler, $\approx 6 - 8$ K, since there are only minor density changes in that region. At central densities $n(H_2) \geq 10^5$, ($t \gtrsim 5.1 t_{ff}$) the e^- abundance at the cloud center is almost entirely due to M^+ , with $X(e^-) = 10^{-8}$. Therefore, at later times the field diffusion rate and cloud evolution is controlled by M^+ . The central M^+ abundance declines slowly with density and during this time the cloud exhibits the same quasi-static behavior while remaining gravitationally stable.

At $t \simeq 5.8 t_{ff}$ the inner core, $r = 0.025$ pc becomes supercritical, although it is still gravitationally stable, $\gamma > 1$, because of the thermal pressure which exceeds the magnetic pressure for $r < 0.05$ pc (fig. 4b). The central density at that time is $n_c = 5.4 \cdot 10^5 \text{ cm}^{-3}$, i.e., 270 times larger than the initial central density, and the central ion fractional abundance at that time is $6.5 \cdot 10^{-9}$. Shortly after that time the quasi-static evolution turns into dynamic collapse for the central regions and the energy ratio drops precipitously. This is accompanied by the corresponding sharp rise in the core density (fig. 5). The collapse phase is followed for $\simeq 0.3 t_{ff}$ within which the peak density rises by more than 6 orders of magnitude, indicating a very rapid dynamical evolution. At the time the inner 0.025 pc core becomes supercritical, $\beta < 1$, larger volumes around the origin are still subcritical, with β at $r = 0.075$ and 0.1 pc being 1.5 and 2.2 respectively. As the dynamic collapse of the core continues, the cloud becomes supercritical at progressively larger radii from its center, with the 0.1 pc volume going for the first time supercritical, $\beta < 1$, at $6.07 t_{ff}$ at $n_c = 4.5 \cdot 10^7 \text{ cm}^{-3}$. The 0.12 pc radius becomes supercritical at $n_c = 2 \cdot 10^9 \text{ cm}^{-3}$ and the 0.145 pc radius at $n_c = 2 \cdot 10^{10} \text{ cm}^{-3}$. At $t \simeq 6.06 t_{ff}$ the inner 0.025 pc lose their thermal support as well and the core becomes gravitationally unstable at $n_c = 8 \cdot 10^6 \text{ cm}^{-3}$, with larger radii about the origin becoming unstable at later times. The supercritical core appears to reach a maximum radius of $\simeq 0.16$ pc, containing $\simeq 6 M_\odot$, at which location it remains to the end of the evolution. Because this happens at central densities close to the termination of the calculation it would be necessary to follow the evolution to even higher densities to confirm that. However given the short timescale of the core evolution towards stellar densities, and that at $r = 0.16$ pc, $n(H_2) = 3 \cdot 10^3 \text{ cm}^{-3}$ and $\tau_v \simeq 3.5$, i.e., field diffusion is slow, we do not expect but a small correction to the eventual size of the supercritical core. In this model, and in the rest in this work, ambipolar diffusion leads to flux redistribution and collapse of the inner cloud core. This conclusion is similar to the behavior exhibited by the models of CM94, CM95 except that the magnetic critical core forms at an earlier stage in the cloud's evolution and at lower central densities. Differences between our models and theirs, that can explain these differences in our results are discussed further below.

Figures 2d, 3d, display the state of the cloud after the inner core becomes subcritical and shortly before it becomes gravitationally unstable and figs. 2e, 3e close to the end of the calculation. The radial velocity for $r < 0.1$ pc remains negative for the remaining of the cloud's

evolution and increases in magnitude up to 1 - 1.5 km s⁻¹. The Mach number increases too; in fig. 2d the maximum Mach number is 0.1 but at the end of the calculation it exceeds 3.5. However the velocity remains always sub-alfvenic. After the central density reaches 10⁶ cm⁻³, OI, CO and OH_x are practically in equilibrium at the core, with fractional abundances changing by no more than 2% as the density increase from 10⁶ to 10¹² cm⁻³, with central values, $X(OI) = 6.8 \times 10^{-5}$, $X(CO) = 10^{-4}$ and $X(OH_x) = 3.2 \times 10^{-5}$. The rapid increase in density also entails a sharp decrease in the abundance of C I, CH_x and C⁺ which are converted into CO, and of the other ions except the metals whose decline is slow. Although the metal abundance at the core, which is essentially the ion abundance, can no longer affect the dynamics of the core it may nevertheless be significant in determining the amount of magnetic flux eventually trapped by the collapsing core. The relative amount of field diffused from the core, $\delta B_{diff}/B$ decreases when the core is in collapse; it is approximately 7×10^{-4} and 4×10^{-5} in figs. 2d and 2e respectively. The amount of magnetic field gained from diffusion from the outer part of the collapsing core is not expected to be important in limiting the total mass of gas that can go into stars by providing further support to the outer collapsing core; at $r \simeq 0.2$ pc at the end of the calculation the ion abundance is still essentially that of C⁺, $\simeq 5 \times 10^{-7}$, which results in a very low diffusion rate. The 6 M_{\odot} may be a lower limit to the actual collapsed mass which can be estimated when following the central density to much higher values, something not feasible with our current numerical resolution. At $n(H_2) > 10^6$ cm⁻³ grain-gas heating is a more dominant heat exchange mechanism than O I cooling and the temperature for $r \leq 0.02$ pc remains at 10 K. For $0.02 \geq r \geq 0.5$ pc the cloud remains even colder, between 6 - 10 K, and only at $r > 0.5$ pc the temperature rises again.

In summary, field diffusion has led to the formation of a collapsing core at a low efficiency, $\simeq 1.5\%$ of the cloud's mass, within a globally stable cloud, whose exterior remains ionized but its core is mostly neutral. The main characteristics of the cloud's evolution under field diffusion, a slow quasi-static contraction followed by a rapid dynamical collapse are the same with past models (refs.) of magnetically subcritical clouds even though the above described model is not magnetically subcritical but overall stable by a combination of magnetic and thermal pressure.

4.2. Dependence on the interstellar radiation field

To examine the influence of the interstellar radiation field in the overall cloud evolution we examine model M4 which is similar to the above model in every respect except that the interstellar radiation field is now restored to its standard value, i.e., an increase in the UV bolometric flux by a factor of 6.3.

In the following we highlight the most important aspects of the cloud's evolution always in comparison to the previous model, M3. The increase in the radiation flux results in a higher UV heating and ionization rate throughout most of the cloud. The initial total thermal energy of the cloud is higher now, with $\alpha = 0.13$ compared to 0.086. The evolution of the cloud is qualitatively the same, with a long quasi-static phase followed by rapid dynamical collapse of the core while the

rest of the cloud remains well supported. The main difference is that the quasi-static phase lasts twice as long here (fig. 5). A comparison between the temperature profiles for the two models, at similar central densities reveals that the temperature in M4 remains higher than in M3 in most of the cloud. For central densities $> 5 \times 10^3 \text{ cm}^{-3}$ in the inner 0.1 - 0.2 pc the temperature profile is very similar for the two models. The reason is that at these higher central densities the enhanced UV extinction ($\tau_v \geq 4$ at 0.1 pc) renders UV heating less effective so temperature variations between the two models are negligible at the central regions. Moving outward from that inner region the temperature in M4 increases monotonically with radius and at the outer boundary the difference is $\approx 25 \text{ K}$. The difference between the two models in the total initial thermal energy within 0.1 pc is no more than 15%; the increase in the cloud's total thermal energy is distributed mostly in the cloud's envelope.

More important for the cloud evolution are differences in the ion abundance, fig. 7. The total ion abundance is again higher in the cloud. Starting from the outer boundary we see that the region of high ion, mostly C^+ , abundance, which in M3 was confined to within $\sim 0.1 \text{ pc}$ from the boundary, is now extended down to a radius of $\sim 0.8 \text{ pc}$ from the origin. The higher ion abundance in the cloud is the result of the increased UV photoinization of C^+ , in most of the envelope, and of M^+ in the cloud center. Even at high central densities, the ion abundance between the two models is the same only in the inner 0.02 - 0.03 pc; e.g., at $n_c = 8 \times 10^4 \text{ cm}^{-3}$ the ratio of the ion abundance of the two models is $\simeq 2$ at the 0.08 pc radius. The immediate consequence of the higher ion abundance is the smaller field diffusion rate which doubles the field diffusion time. Apart from the longer evolutionary timescale, when we compare the two models at the same central densities the profiles of density, and magnetic field with radius are very similar, while the profiles of the chemical species exhibit differences of the same relative level with the total ion abundance.

The cloud becomes supercritical, although gravitationally stable, in its inner core, $r = 0.025 \text{ pc}$, at $t \simeq 11.4 t_{ff}$ with $n_c = 2.8 \times 10^5$, a ratio of 140 with respect to the initial central density, and it becomes unstable at $t = 12.3 t_{ff}$, with $n_c = 1.7 \times 10^6 \text{ cm}^{-3}$. As in M3 a supercritical core grows rapidly to its maximum radius. At the end of the computation the inner $\simeq 0.14 \text{ pc}$ are supercritical and in dynamical collapse, containing $\simeq 4.5 M_\odot$. The small mass difference contained in the supercritical core between the two models is probably related to the slower diffusion rate of M4 at 0.1 - 0.2 pc although evolution towards larger densities and higher numerical resolution would be necessary for a definite comparison.

These results, that an increased ambient UV flux increases the field diffusion time, appear to be in contrast with those of CM95. These authors compare models with and without the UV field and find that the UV models evolve faster. There are many differences in our models and theirs, however, that cannot allow a direct comparison. CM95 model what in reality is a relatively oblate cloud as an infinitesimally thin disk to study evolution in the radial direction via ambipolar diffusion whereas a typical oblate cloud in our work is approximated as a sphere. Even though their model cloud is less massive, $98 M_\odot$, the initial optical depth in the radial direction at the

cloud center is much greater than in our models, > 10 , because a two-dimensional disk of that mass poses a much larger column density in the radial direction than a sphere of comparable mass. The result is that in CM95 only the cosmic-ray flux contributes to the ionization rate at the cloud center, whereas the UV can become important only in the cloud envelope and decrease the diffusion rate at the envelope. In our model however the UV affects the ionization rate at the cloud center for most of the cloud’s evolution, at the same time rendering field diffusion at the envelope insignificant. That leads, in CM95, to the indirect UV effect of the dilution of the envelope’s gravitational effect on the core and the more rapid core collapse in the presence of UV. Both results are therefore valid, since they are derived from a different set of parameters.

4.3. Dependence on the cosmic-ray ionization rate and metal abundance

In model M5 we examine the effects of increasing both the cosmic-ray ionization rate and the initial metal abundance, while keeping everything else the same as in M3. The values $\zeta_p(H_2) = 5 \times 10^{-17} \text{ s}^{-1}$ and $[M]/[n(H_2)] = 10^{-7}$, are at the high end of their observationally determined range and are expected to allow the longest possible diffusion time compared to M3.

The primary effect of the higher cosmic-ray flux on the cloud dynamics is the direct increase in the production of H_3^+ and He^+ , and the indirect increase of the abundance of the other ions through ion-molecule reactions and the charge transfer reaction for the metals, which reduces the field diffusion rate. A secondary effect is the increase of the gas temperature, resulting from the higher cosmic-ray heating term. Similarly, the higher metal abundance significantly decreases the field diffusion rate at later stages of the evolution, when M^+ is the dominant ionic species.

The net result is a long diffusion timescale with the inner core becoming supercritical at $\simeq 28.4 t_{ff}$ with $n_c = 10^6 \text{ cm}^{-3}$. The interval where C^+ is the dominant ionic species extends now to $18 t_{ff}$, when $X(C^+) \simeq X(M^+)$ at the core, compared to $2.5 t_{ff}$ in M3. Although the abundance of the other three ions is now higher at the core, the larger value of $X(M^+)$ renders their contribution to the total ion abundance at the core insignificant at all times. At central densities $n(H_2) > 2 \times 10^4 \text{ cm}^{-3}$, $t \simeq 23 t_{ff}$, M^+ is the only significant contributor to the ion abundance at the cloud center. As in M3 at radii $r \geq 0.13 \text{ pc}$ $X(C^+) \simeq X(e^-)$, except at the outer boundary where $X(He^+)$ can exceed $X(C^+)$. A comparison of the fractional ion abundances at the same central densities between the two models will show that at any instant during the cloud’s evolution the fractional ion abundances are the same at the outer boundary but moving inwards M5 shows a monotonically increasing higher ion abundance with decreasing radius compared to M3. The largest difference is at the core; at central densities $2.5 \cdot 10^3$ and $8 \cdot 10^4 \text{ cm}^{-3}$ the ratio of the ion fractional abundances of the two models at the center is $\simeq 5$ and 7 respectively. The core becomes supercritical at $28.4 t_{ff}$ with $n_c = 10^6 \text{ cm}^{-3}$ and when it becomes unstable, at a central density of $1.3 \cdot 10^6 \text{ cm}^{-3}$, $X(e^-) = 3 \times 10^{-8}$ at the cloud center, which is a factor of 11 larger than the corresponding value of M3 when it becomes unstable.

The collapsing supercritical core extends up to $\simeq 0.12$ pc, containing $\simeq 5.7 M_{\odot}$, which is close to the core mass in M3 and larger than in M4. Despite the smaller radius of the core, compared to M4, the core mass is higher because the cloud evolves for a longer time and the core forms at higher central densities. Although a better numerical resolution will be necessary to make conclusive statements regarding how the variation in the UV field as compared to initial ionic abundance affects the core properties, we can already see a trend here; larger initial ionic abundance or UV both increase the time evolution but the former tends to result in a more compact core than the latter.

4.4. Lower density isolated clouds

Here we examine a series of diffuse isolated clouds, such as a lower density version of model M4, subject to irradiation from the full interstellar UV field. Similar thermally supported clouds we studied by NL97 and found to collapse via molecular cooling. The central regions of diffuse clouds are expected to have higher fractional ionization than in the models previously examined, rendering field diffusion slow, while their outer parts are subject to photoevaporation from the ambient UV field. The main issue in studying low density clouds is whether they can evolve towards higher densities via field diffusion of a scalar field, and the relative evolution timescale as a function of central density.

We constructed three $400 M_{\odot}$ models with average central densities, 400 (model M1), 750 (M2) and 1400 cm^{-3} (M6). One of the issues in the construction of initial states for the low density clouds with thermal cooling is that stable states, in the absence of field diffusion, exist when the ratio of magnetic to potential energy is above a certain range. The reason is that the initial value of α in these models can be close to the stability limit (≈ 0.5) for thermally supported clouds. It would appear then that these clouds can become stable with only a small amount of magnetic flux added. Cooling, however, can render these clouds locally unstable when, for example, they reach transitory higher local densities during their relaxation to equilibrium and ultimately the cloud will collapse. A significant amount of magnetic flux, $E_m \sim E_{th}$ has to be added to the cloud in order to keep the central density from fluctuating towards much higher values during transition to equilibrium. This is not the case for denser clouds where the thermal energy is a small contribution to the total energy of the cloud. For that reason, in these three models the ratio of the magnetic energy to potential energy is not the same, and we do not perform a detailed evolutionary comparison.

The evolution of central density with time for the three models is shown in fig. 10, where the trend of shorter quasi-static evolution time for higher initial central densities is clearly evident. The evolution of M1 is extremely slow and is followed for up to $\simeq 165$ Myr ($50 t_{ff}$), at which time the central density has reached $\simeq 1500 \text{ cm}^{-3}$. The fractional ion abundance at the cloud center has reached 2×10^{-6} , mostly in the form of C^+ and $\tau_v \simeq 1.5$. The evolution of M2 is somewhat faster, with $n_c \simeq 10^4 \text{ cm}^{-3}$ after 95 Myr. From the apparent linear dependence of the log of

density with time in fig. 10, a considerably longer time, ~ 150 Myr is required for M2 to reach 10^5 cm^{-3} central densities. In M1 the rate of field diffusion is approximately a factor of 10 smaller than that of M6, which becomes unstable at 32.5 Myr ($17.5 t_{ff}$). At the end of the computation the unstable core in M6 extends up to 0.17 pc from the center, containing $\simeq 5 M_{\odot}$.

Because the density at the outer cloud boundary is now low, $10 - 30 \text{ cm}^{-3}$, the outer cloud layers are heated to temperatures higher than in the denser clouds, $\simeq 100 - 120 \text{ K}$. As a result they are subject to an outward expansion which is only inhibited by the external confining pressure. As mentioned elsewhere the external pressure on the cloud is set equal to the total of the outer portions of the cloud, on the assumption that the density, magnetic field and temperature in the medium exterior to the cloud will not differ substantially from their values at the cloud boundary. The lack of modeling of the cloud boundary with the surrounding medium does not allow us to study the degree of photoevaporation and the mass-loss of the warm halos for these low density clouds. The fact however that low density clouds, $n(H_2) \leq 750 \text{ cm}^{-3}$, require $> 100 - 200$ Myr to evolve to high densities indicates that they are much more likely to dissipate via photoevaporation and not be observed to enter the star formation phase. consequence of the ambient UV field which maintains a high ion abundance in the cloud centers.

We remark that the choice of cosmic-ray flux and initial metal abundance are those that will produce the shortest possible field diffusion timescale. As we have seen from earlier discussions, an increase in the values of these parameters closer to the high-end of their range would increase their evolution time by a factor ~ 4 , thereby strengthening the argument that such low density magnetically supported isolated clouds photoevaporate before they can collapse via field diffusion across field lines.

5. Comparison with previous calculations

Our modeling procedure of ambipolar diffusion appears to capture well the essentials of cloud collapse via flux redistribution. The cloud evolves quasi-statically until the innermost core first becomes supercritical, and then contraction within the supercritical core continues on a dynamical timescale. The results are physically meaningful under parameter variation: an increase in the external UV field, initial metal abundance or a decrease of the central cloud density tend to increase t_{ad} . Here we make some comparisons between our results and those of CM95 which represent the most detailed models of past work on this subject.

Overall there is good qualitative agreement but there are many differences in the geometry, initial conditions including initial abundances, magnetic modeling and chemical network between the two models, that can explain some of the differences in the results. One of the key differences is the assumption of the cloud's morphology; disk vs sphere. The large column densities in the radial direction in CM95 result in a large initial value of τ_v at the cloud center, ≥ 10 , so that UV radiation affects the cloud's envelope and the main ionizing agent at the cloud core is the

cosmic-ray flux. In contrast, in our models the UV field is dominant at the core initially, $\tau_v \leq 2$, and for a significant fraction of the cloud's evolution. While the UV field is dominant initially in the cloud core a decrease in the level of UV will substantially decrease t_{ad} ; a 2 magnitude UV extinction at the cloud boundary will decrease t_{ad} by a factor of $\simeq 2$. When τ_v is large at the cloud core initially, inclusion of the UV field will lead to a better support of the cloud's envelope and actually decrease t_{ad} (CM95).

In both works the increase of the central density is slow until the core becomes supercritical at which point dynamic collapse sharply raises n_c with time. In the UV models of CM95 the central mass-to-flux becomes critical when the central density has increased by a factor ≈ 30 compared to the initial central density, i.e., at $n_c \approx 8 \cdot 10^4 \text{ cm}^{-3}$. In contrast in our models, except M5 which has different parameters (see Table 1), the central region becomes supercritical at densities $2 \cdot 10^5 - 5.5 \cdot 10^5 \text{ cm}^{-3}$, i.e., larger than the initial central density by a factor 140 - 270. In both works, shortly after the central region becomes supercritical, a supercritical core forms, extending up to a certain fixed radius. In CM95 the core has fully formed while $n_c < 10^5 \text{ cm}^{-3}$, in our models however the supercritical core has fully formed when $n_c > 10^{10} \text{ cm}^{-3}$, i.e., very close to termination of the computation. This is attributed mainly to the different cloud geometries which admit different initial conditions for static or quasi-static configurations. In both works the initial density profile is non-uniform but the initial equatorial field component in CM95 (fig. 6d) is uniform whereas ours decreases with radius as $B \sim \rho^{2/3}$. As a result the initial mass-to-flux profile in CM95 (e.g., fig 6a) decreases with radius whereas in our models increases with radius. Furthermore, the central initial mass-to-flux value in CM95 is 0.256 and in our models is $\simeq 0.05$, i.e., a factor of 5 smaller than in CM95. In other words the relative magnetic support of the central region is stronger in our model than in CM95, but the converse is true for the cloud envelope. As a result a larger relative amount of magnetic flux, compared to CM95, has to diffuse from the core in order to render it supercritical, and as a consequence the gravity at the core will dominate the magnetic support only at higher densities.

The mass contained in the supercritical cores is 1 - 1.5 % of the cloud mass, whereas in the UV models of CM95 the supercritical core is $\simeq 5 - 6$ % of the cloud mass, i.e., we find star formation via ambipolar diffusion to be less efficient than CM95. This result is a consequence of the central region becoming supercritical at high densities and of the relatively low UV extinction, which essentially determines the radius of the supercritical core to be confined between 0.1 - 0.2 pc where, $\tau_v \sim 3 - 4$, the ion fractional abundance is relatively high, $X(e^-) \simeq X(C^+) \approx 10^{-7}$ and the diffusion rate minimal. During core formation, at the radius of the supercritical core $n(H_2) \approx 3 - 5 \cdot 10^3 \text{ cm}^{-3}$, so that depletion of C^+ onto grains, which is not included in our model, is very slow and its overall effect at increasing the core radius and mass will be small.

6. Conclusions and summary

This work comprises the first effort to include ambipolar diffusion in an SPH formulation with the eventual goal of studying cloud collapse and fragmentation by incorporating in a three-dimensional model dynamical, thermal, chemical, radiative and magnetic effects. The magnetic field is modeled as a scalar, in an approximation that neglects the magnetic tension, as a first step towards building more self-consistent models. A natural consequence of that approximation is that clouds are assumed to be spherical instead of the more general prolate morphologies that they are observed to be. The conclusions that we draw here for spherical clouds can also be regarded as valid for actual non-spherical clouds for collapse across field lines, or when there's significant field tangling on short scales to avoid cloud collapse along field lines. Below we summarize our most important results.

The ambipolar diffusion timescale, t_{ad} , was found to be a sensitive function of the central density, UV field and initial ion abundance. In order for a supercritical core to form within a few $\times 10^7$ years the central density must exceed 10^3 cm^{-3} . Low density isolated clouds require more than 10^8 years to raise their central density by 1 - 2 orders of magnitude. We expect that these clouds do not collapse via ambipolar diffusion if the magnetic field is significant for their support, i.e., if they are either subcritical or supercritical but with magnetic energy comparable to their thermal energy. One possible exception is if they are compressed by some external triggering mechanism such as cloud-cloud collision or the passage of shock waves, which may increase the core density to the point where ambipolar diffusion removes the field at a rapid rate.

The interstellar UV field is important in determining the ion abundance at the cloud center for a large fraction of the cloud's evolution. For initial central densities in the $10^2 - 10^3 \text{ cm}^{-3}$ range and UV fields within a few magnitudes of the standard interstellar values the rate of field diffusion is controlled mainly by the external UV field. For that reason the ratio of t_{ad} to free-fall time is not constant as would be expected for ionization mainly from cosmic-rays (McKee et al. 1993). Otherwise identical clouds, located in regions of differing extinction will evolve on different timescales. Our results on the effects of the UV in cloud evolution are in agreement with those of Jessop & Ward-Thompson (2000) from far-infrared surveys of cloud cores, who find consistency in the relation between lifetime and ionization levels of cloud cores. Elaborate and mention McKee 1989 where core formation is regulated by external radiation.

As found by past works on the subject, star formation via ambipolar diffusion is a process of low efficiency; only 1 - 1.5 % of the total cloud mass becomes gravitationally unstable and collapses. Since, however we have not varied the mass of the clouds in our models, scaling of efficiency with cloud mass is not known. By extrapolating to lower mass clouds with the same magnetic to gravitational energy ratio and similar initial central densities and other parameters we would expect a lower column density and therefore extinction to the cloud center and as a result a longer t_{ad} than we find for $400 M_{\odot}$ clouds.

Nikos Mastrodemos is a National Research Council Research Associate. This research was conducted at the Jet Propulsion Laboratory, California Institute of Technology, under support from the National Aeronautics and Space Administration.

Table 1. Cloud model parameters

Model	Mass (M_{\odot})	Radius (pc)	n_c (cm^{-3})	B_c (μ G)	γ	E_m/E_g	E_{th}/E_g	G_o
M1	400	2.5	400	9.5	2.2	0.4	0.51	1
M2	400	2.5	750	12.9	1.98	0.32	0.51	1
M3	400	1.35	2000	30.5	1.6	0.48	0.08	0.16
M4	400	1.35	2000	30.5	1.7	0.48	0.13	1
M5 ^a	400	1.35	2000	30.5	1.62	0.48	0.09	0.16
M6	400	1.725	1400	22	1.67	0.41	0.22	1

^a $\zeta_p(H_2) = 5 \times 10^{-17} s^{-1}$, $[n(M)]/[n(H_2)] = 10^{-7}$

Table 2. Cloud model results

Model	t_{ad} (t_{ff})	t_{ad} (Myr)	M_{core} (M_{\odot})	r_{core} (pc)
M1	$\gg 50$	$\gg 160$	-	-
M2	$\gg 40$	$\gg 120$	-	-
M3	5.76	7.48	6	0.16
M4	11.43	14.84	4.5	0.14
M5	28.37	36.84	5.7	0.12
M6	17.1	32.1	5	0.17

REFERENCES

- Basu, S., and Mouschovias, T.Ch. 1994, *ApJ*, 432, 720
- Basu, S., and Mouschovias, T.Ch. 1995, *ApJ*, 453, 271
- Bergin, E.A., Plume, R., Williams, J.P., and Myers, P.C. 1999, *ApJ*, 512, 724
- Boss A.P., 1997, *ApJ*, 483, 309
- Brookshaw, L. 1985, *Proceedings of the Astronomical Society of Australia*, 198, 6, 461
- Chandrasekhar, 1961, *Hydrodynamic and Hydromagnetic stability*, p. 577, Oxford University Press
- Ciolek G.E., and Mouschovias, T.Ch. 1993, *ApJ*, 418, 774
- Ciolek G.E., and Mouschovias, T.Ch. 1994, *ApJ*, 425, 142 (CM94)
- Ciolek G.E., and Mouschovias, T.Ch. 1995, *ApJ*, 454, 194 (CM95)
- Contopoulos, I., Ciolek, G.E., and Königl, A. 1998, *ApJ*, 504, 247
- Crutcher, R.M., Troland, T.H., Goodman, A.A., Heiles, C., Kazès, I., and Myers, P.C. 1993, *ApJ*, 407, 175
- Crutcher, R.M., Roberts, D.A., Mehringer, D.M. and Troland, T.H. 1996, *ApJ*, 462, L79
- Crutcher, R.M., Troland, T.H., Lazareff, B., Paubert, G., and Kazès, I. 1999, *ApJ*, 514, L121
- Crutcher, R.M. 1999, *ApJ*, 520, 706

Fiedler, R.A., and Mouschovias, T.Ch. 1993, ApJ, 415, 680

Gingold, R.A., and Monaghan, J.J. 1977, MNRAS, 181, 375

Goldsmith, P.F., and Langer W.D. 1978, ApJ, 222, 881

Goodman, A.A., Crutcher, R.M., Heiles, C., Myers, P.C., and Troland, T.H. 1989, ApJ, 338, L61

Güsten, R., Fiebig, D., and Uchida, K.I. 1994, A&A, 286, L51

Hernquist, L., and Katz, N., 1989, ApJS, 70, 419

Jessop, N.E., and Ward-Thompson, D., 2000, MNRAS, 311, 63

Langer, W.D. 1978, 225, 95

Li, Z.-Y, and Shu, F.H. 1997, ApJ, 475, 237

Li, Z.-Y, 1998, ApJ, 493, 230

Li, Z.-Y, 1998, ApJ, 497, 850

Lizano, S., and Shu, F.H. 1989, ApJ, 342, 834

Lucy, L.B. 1977, AJ, 82, 1013

Mac Low, M.-M., 1999, ApJ, 524, 169

Mestel, L. and Spitzer, L.Jr. 1956, MNRAS, 116, 503

McKee, C.F., 1989, ApJ, 345, 782

- McKee, C.F., Zweibel, E.G., Goodman, A.A., and Heiles, C., 1993, *Protostars and Planets III*, p. 327, E.H. Levy and J.I. Lunine, eds.
- Millar T.J., Farquhar, P.R.A., and Willacy, K. 1997, *A&AS*, 121, 139
- Monaghan, J.J. 1992, *ARA&A*, 30, 543
- Mouschovias, T.Ch. 1976, *ApJ*, 207, 141
- Mouschovias, T.Ch., and Spitzer, L.Jr. 1976, *ApJ*, 210, 326
- Mouschovias, T.Ch. 1979, *ApJ*, 228, 475
- Mouschovias, T.Ch. 1991, *ApJ*, 373, 169
- Myers, P.C., and Goodman, A.A. 1988, *ApJ*, 326, L27
- Myers, P.C., and Goodman, A.A. 1988, *ApJ*, 329, 392
- Myers, P.C., Fuller, G.A., Goodman, A.A., and Benson, P.J. 1991, *ApJ*, 376, 561
- Nakano, T. 1979, *PASJ*, 31, 697
- Nakano, T. 1983, *PASJ*, 35, 209
- Nelson, R.P., and Papaloizou, J.C.B. 1994, *MNRAS*, 270, 1
- Nelson R.P., and Langer W.D. 1997, *ApJ*, 482, 796, (NL97)
- Nelson, R.P., and Langer, W.D. 1999, *ApJ*, 524, 923, (NL99)

- Neufeld, D.A., and Kaufman M.J. 1993, ApJ, 418, 263
- Neufeld, D.A., Lepp, S., and Melnick, G.J. 1995, ApJS, 100, 132
- Ostriker, E.C., Gammie, C.F., and Stone, J.M. 1999, ApJ, 513, 259
- Paleologou, E.V., and Mouschovias, T.Ch. 1983, ApJ275, 838
- Roberts, D.A., Crutcher, R.M., Troland, T.H., and Goss, W.M. 1993, ApJ, 412, 675
- Ryden, B.S. 1996, ApJ, 471, 822
- Safer, P., McKee, C.F., and Stahler, S.W. 1997, ApJ, 485, 660
- Strittmatter, P.A 1966, MNRAS, 132, 359
- Sundstrom et al., 1993, Science
- Tomisaka, K., Ikeuchi, S., and Nakamura, T. 1988, ApJ, 335, 239
- Tomisaka, K., Ikeuchi, S., and Nakamura, T. 1990, ApJ, 363, 202
- Troland, T.H., Crutcher, R.M., Goodman, A.A., Heiles, C., Kazès, I. and Myers, P.C. 1996, ApJ, 471, 302
- Williams, J.P., Bergin, E.A., Caselli, P., Myers, P.C., and Plume, R. 1998, ApJ, 503, 689

Fig. 1.— Comparison of the predicted total electron abundance in a cloud interior between our chemical network and the UMIST stand-alone chemical code.

Fig. 2.— Figure 2, a-e. Model M3. Radial profiles of the number density of molecular hydrogen (top left), the magnetic field (solid line) and the gas temperature (dotted line), top right, the radial component of the gas velocity (bottom left) and the magnetic field diffused at that particular instant (bottom right). Density units are in cm^{-3} , velocity units are in $km\ s^{-1}$ magnetic field units are in μ Gauss and length units in log pc. Time in free-fall units and years is in the top left.

Fig. 3.— Figure 3, a-e. Model M3. The radial profiles, at the same time as in figure 2, of the fractional abundances of the ten species of the chemical network and the e^- fractional abundance. The left panel displays the neutral species and the right panel the ions. Length units are in log pc.

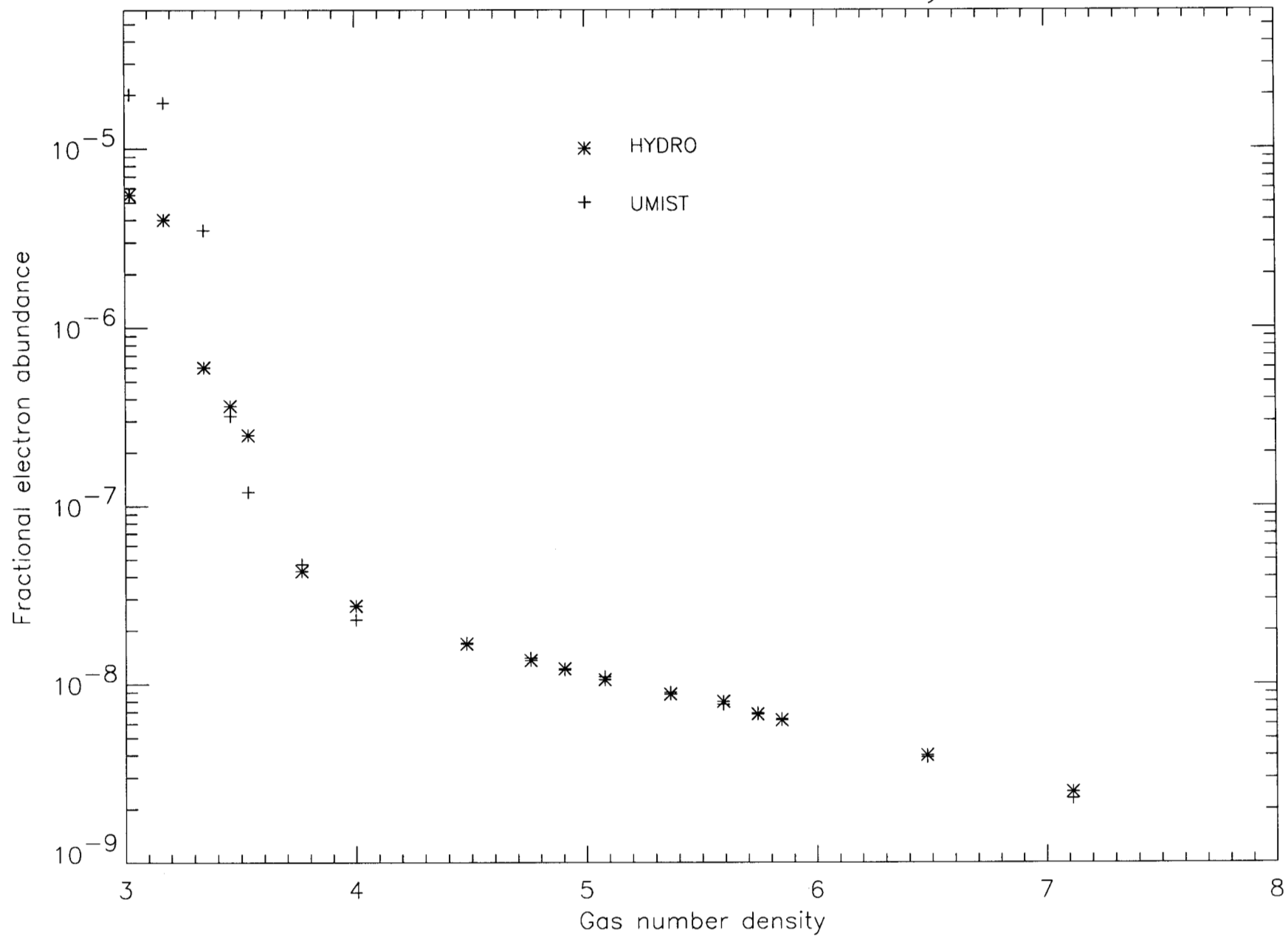
Fig. 4.— Figure 4a. Time evolution of the energy ratios for model M3 for the whole cloud. Figure 4b. Time evolution of the following quantities: Left panel; ratio of total to potential energy, central panel: mass within the enclosed volume, right panel: ratio of magnetic to potential energy (solid line) and thermal to potential energy (dotted line) for the innermost 0.1 pc volume (upper row) and 0.025 pc volume (lower row). Time is in units of free-fall time.

Fig. 5.— Time evolution of the central cloud number density for models M3 and M4 Density is in cm^{-3} and time in free-fall units.

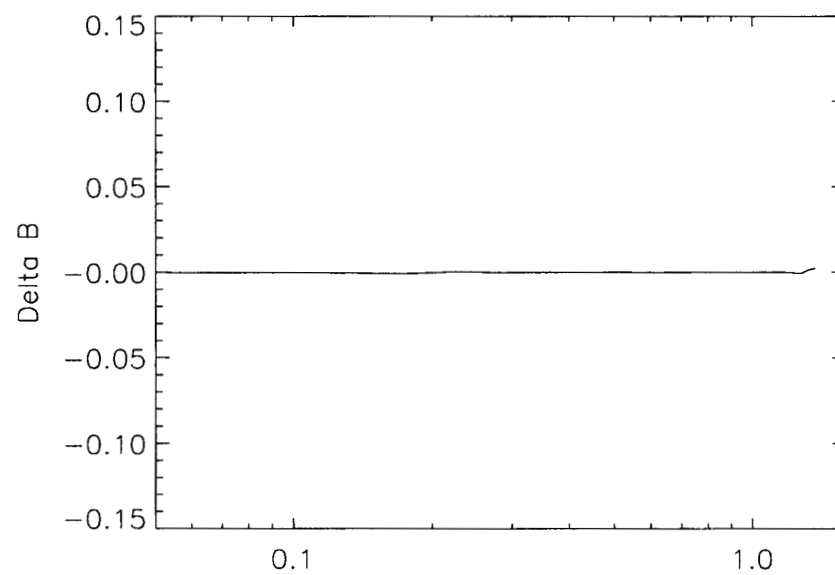
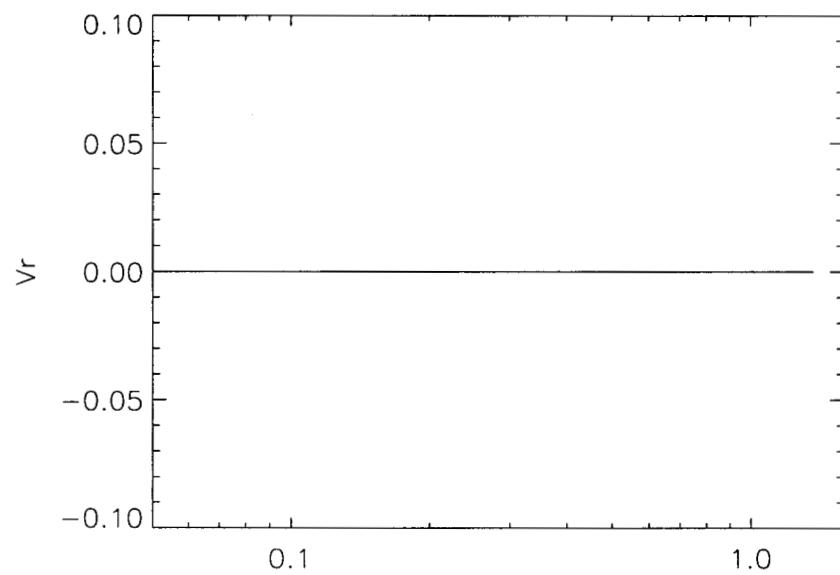
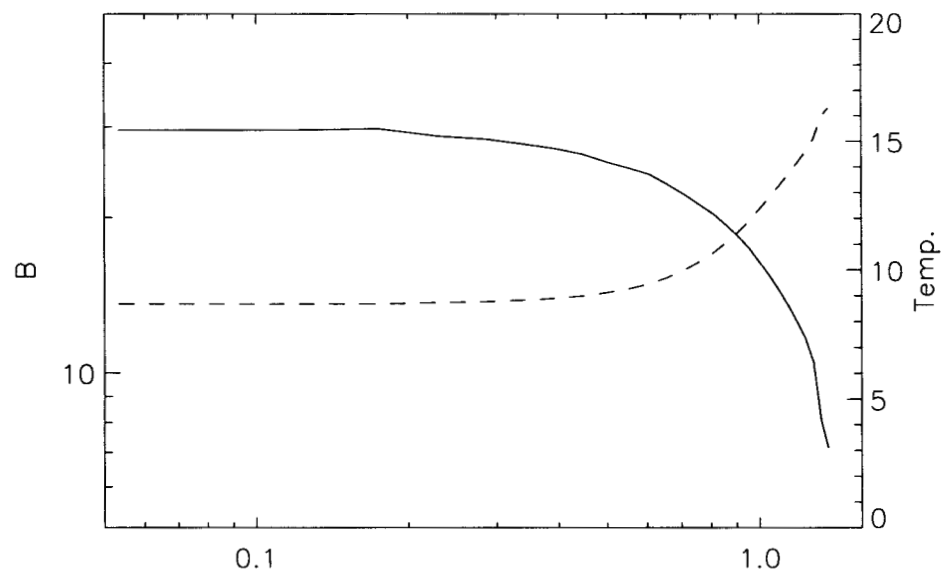
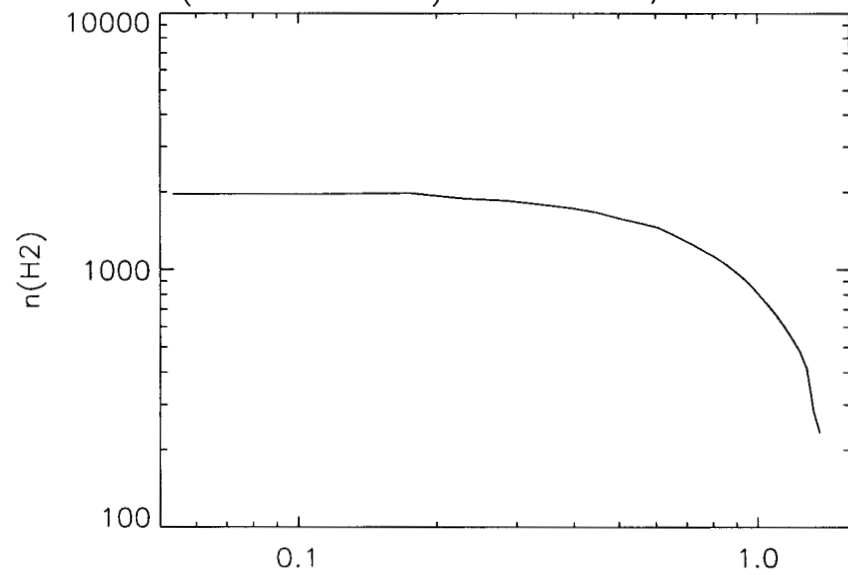
Fig. 6.— Comparison of the radial profiles of the total ion fractional abundance between model M4 (Solid line) and M3 (dotted line), at the indicated 3 different central number densities.

Fig. 7.— Comparison of the central density evolution vs. time for models M1, M2, M6 and M4. Time is in 10^6 years and density in cm^{-3} .

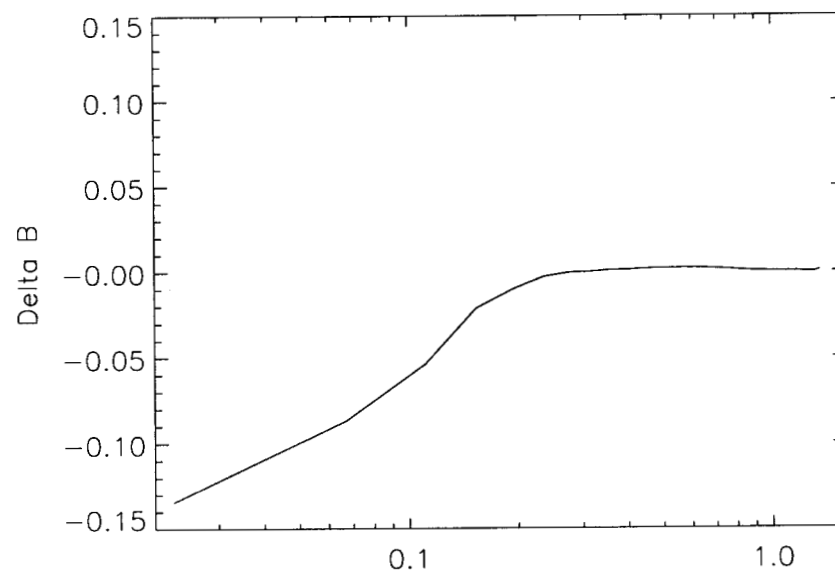
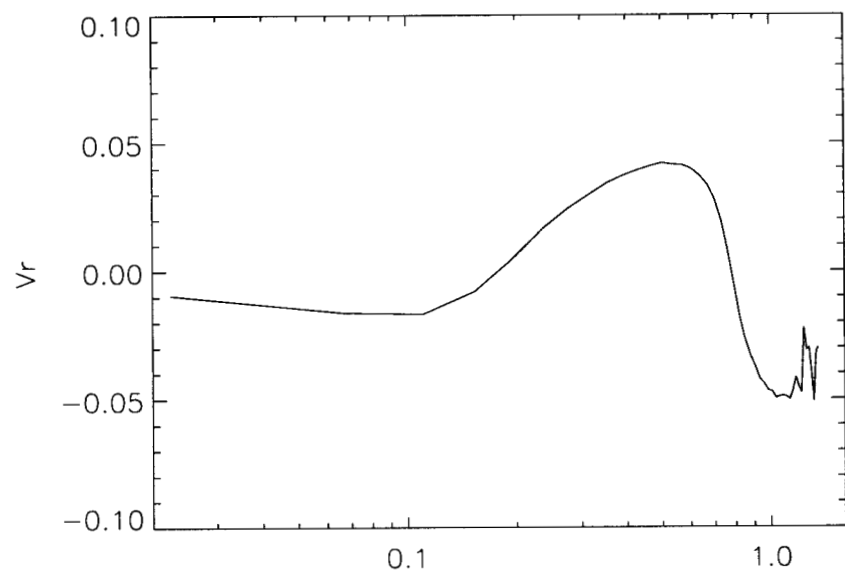
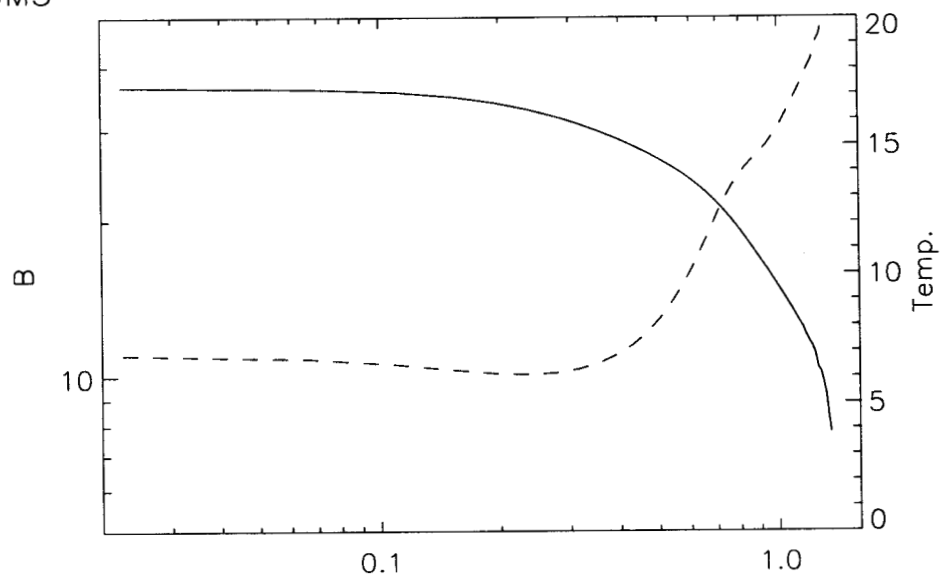
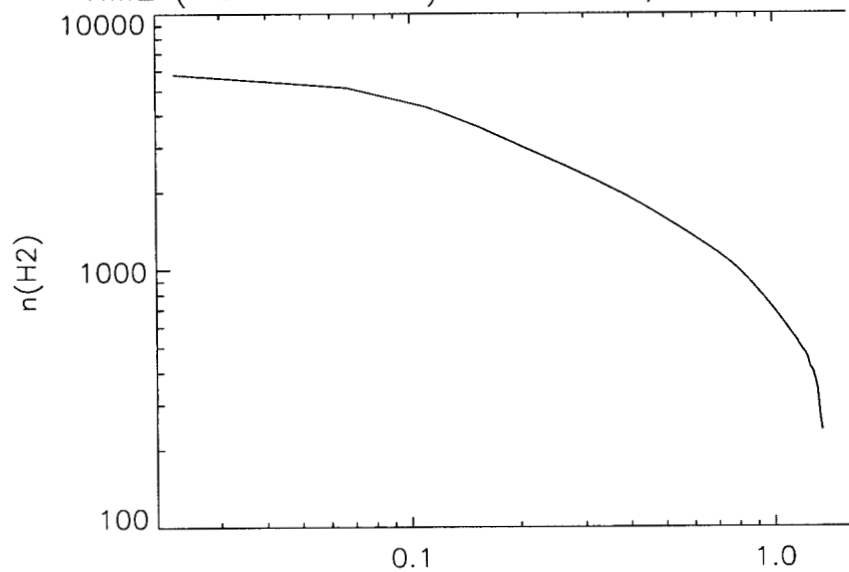
Total e- abundance vs. density



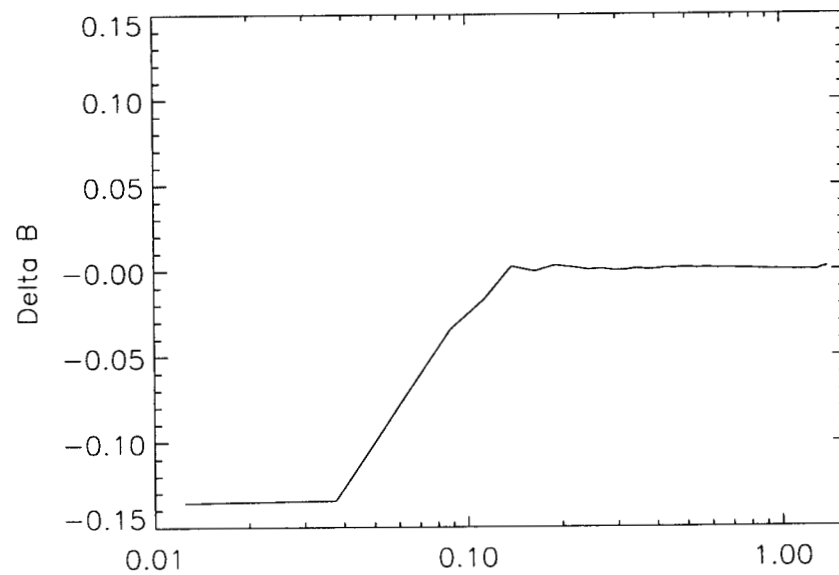
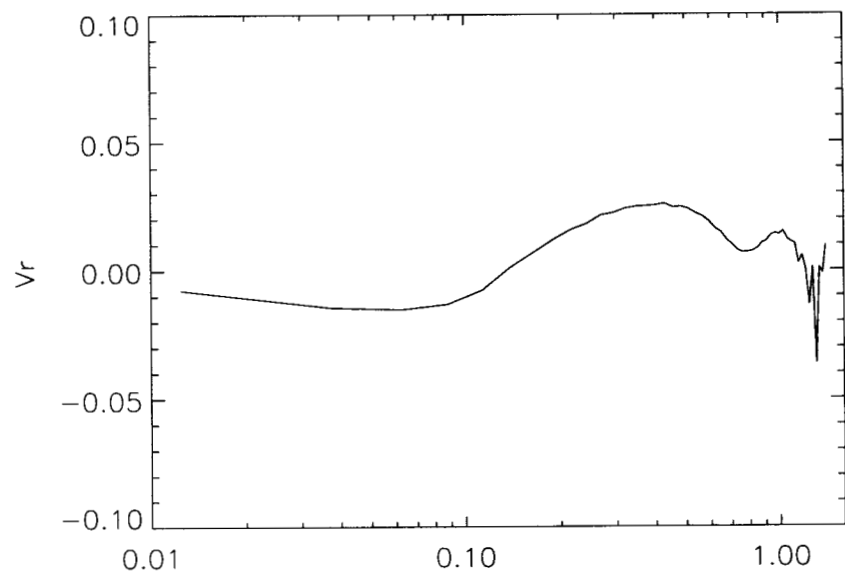
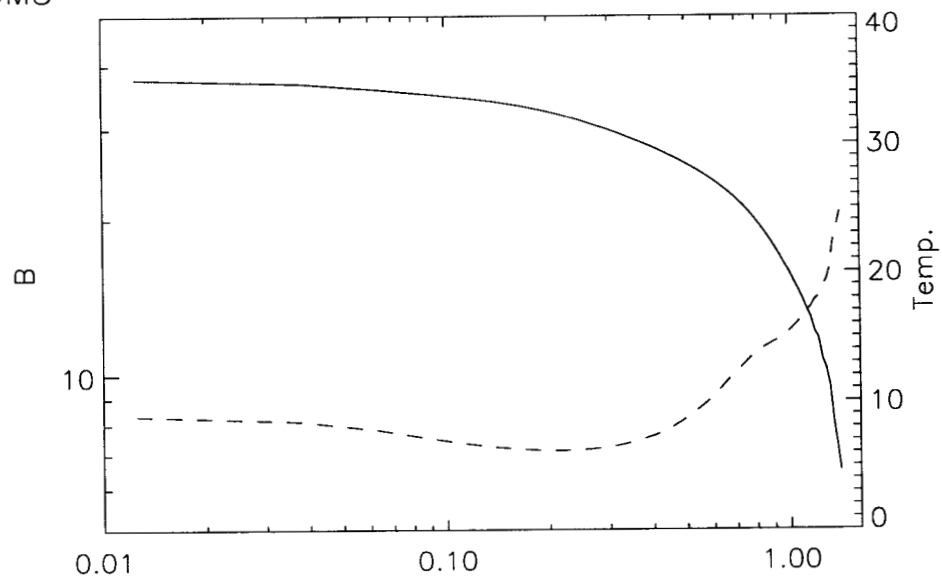
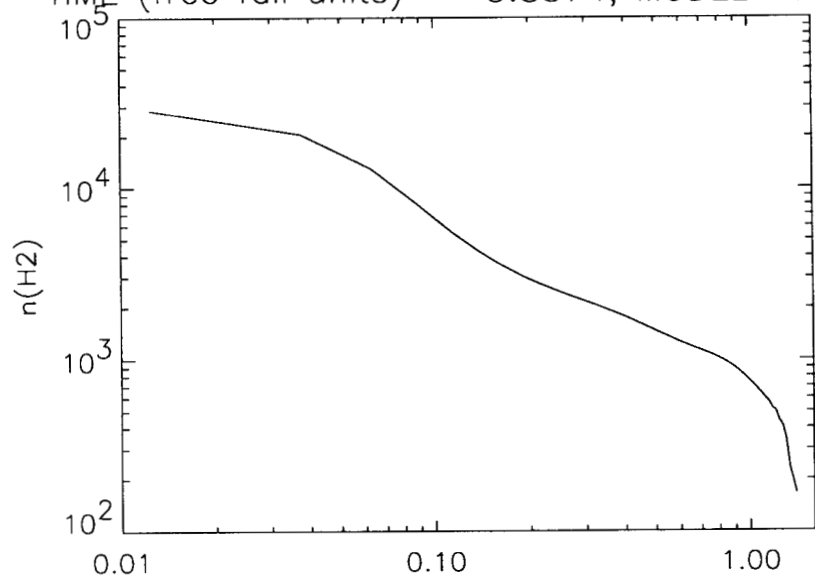
TIME (free fall units) = 0.0043, MODEL 400M3



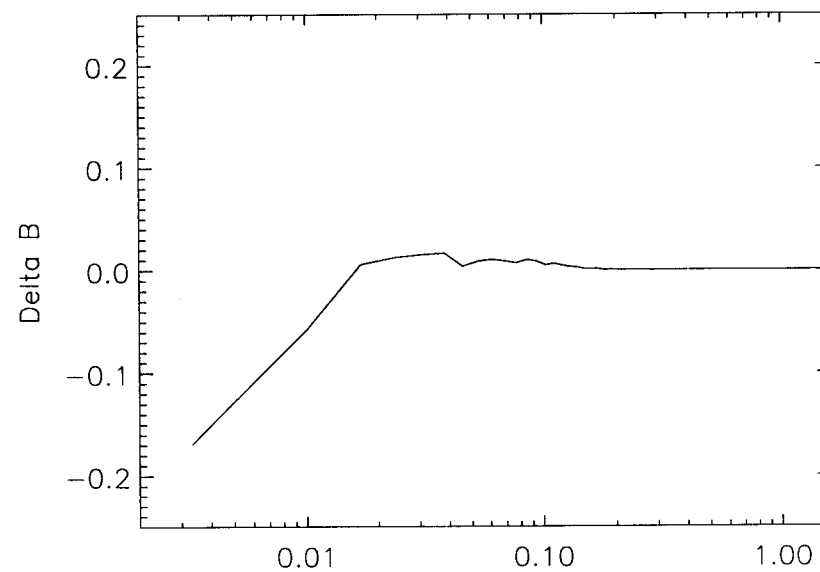
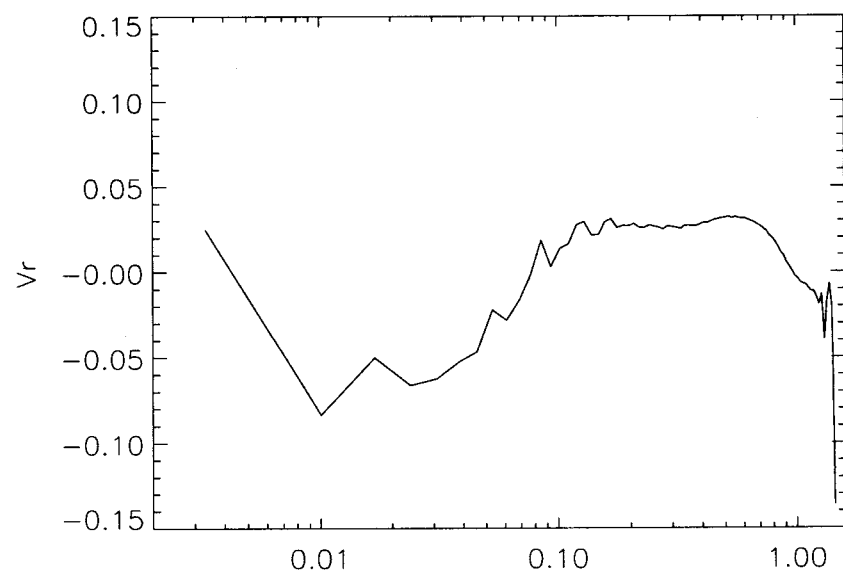
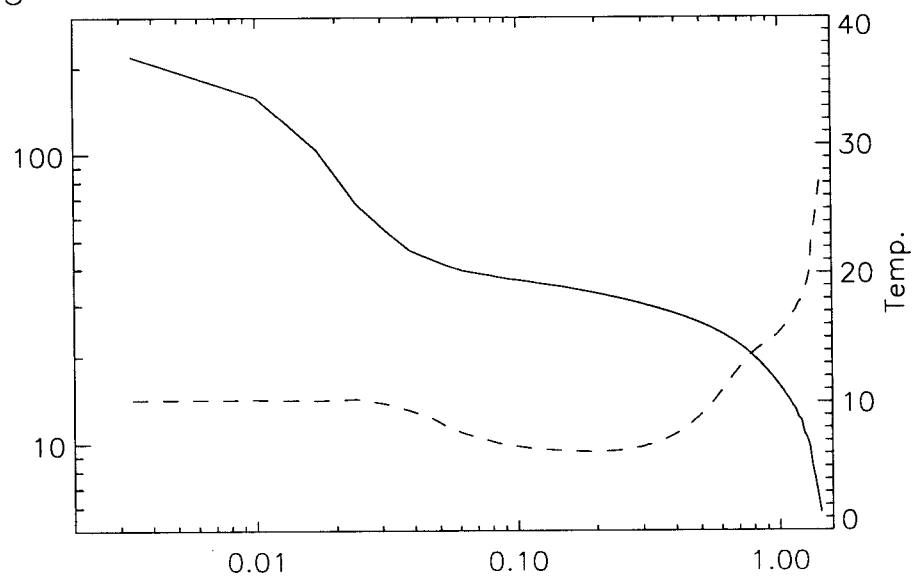
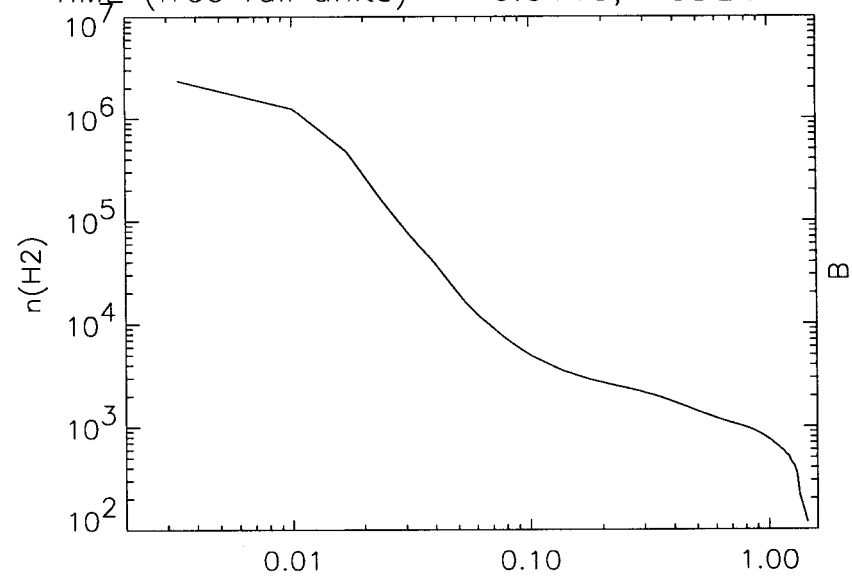
TIME (free fall units) = 2.2417, MODEL 400M3



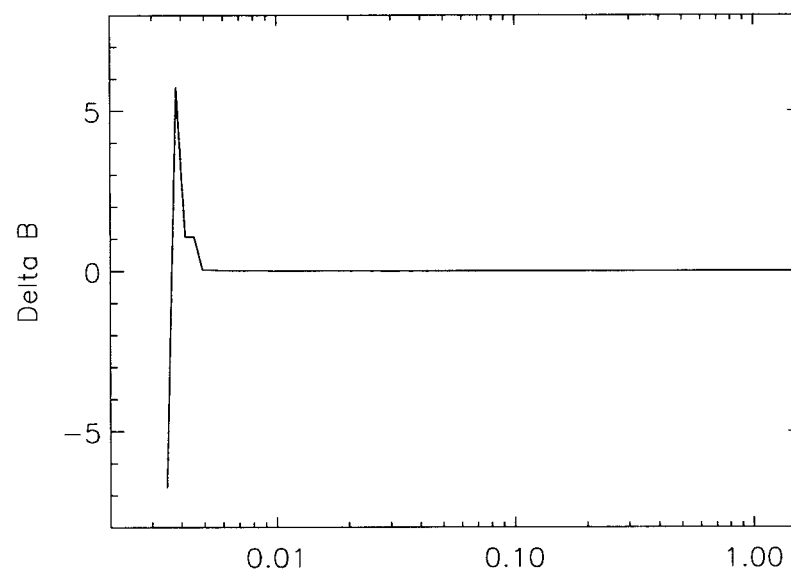
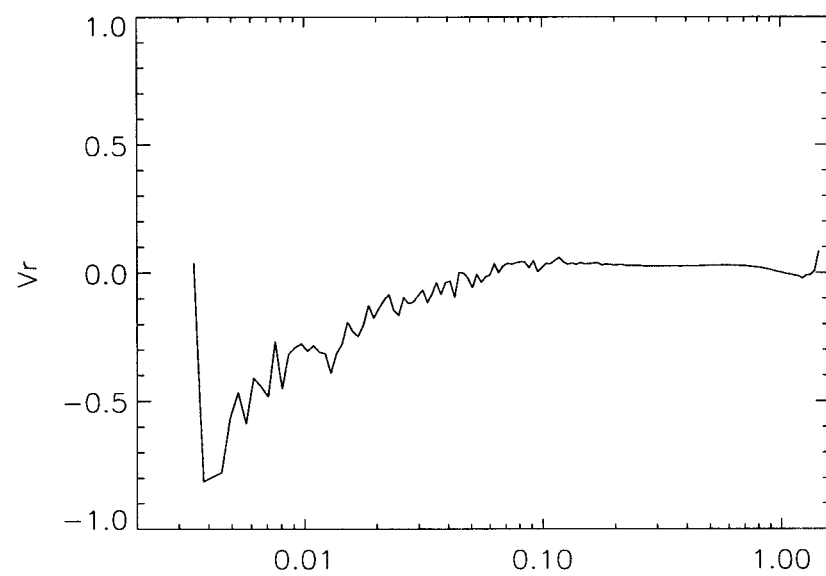
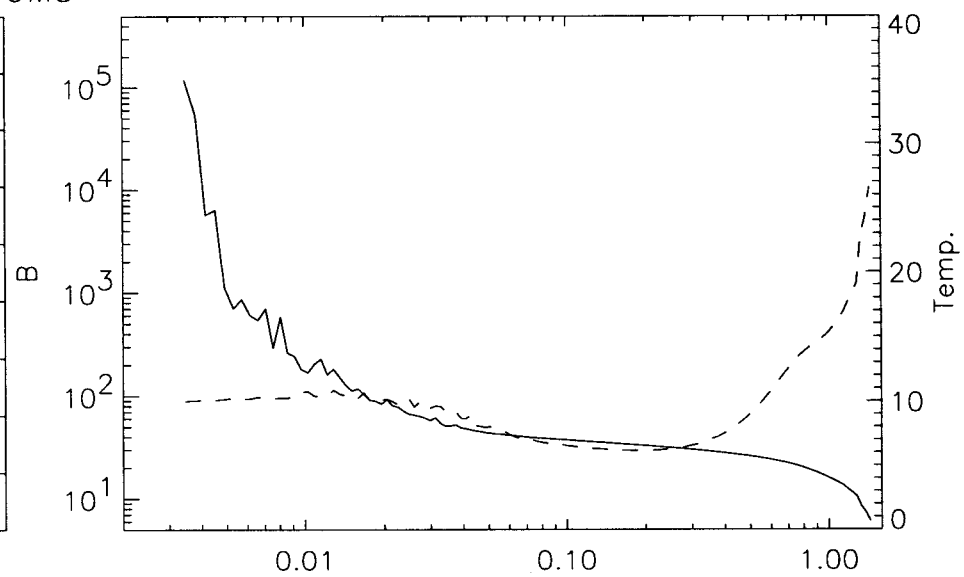
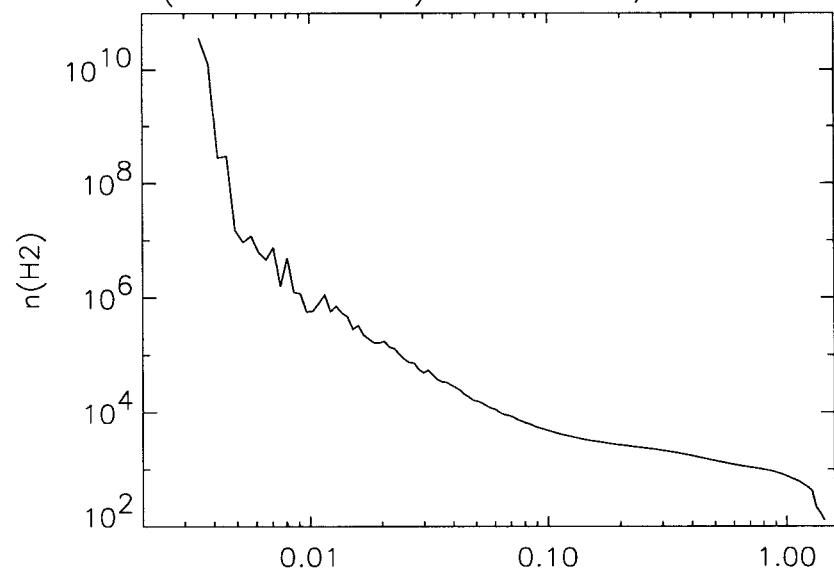
TIME (free fall units) = 3.8574, MODEL 400M3



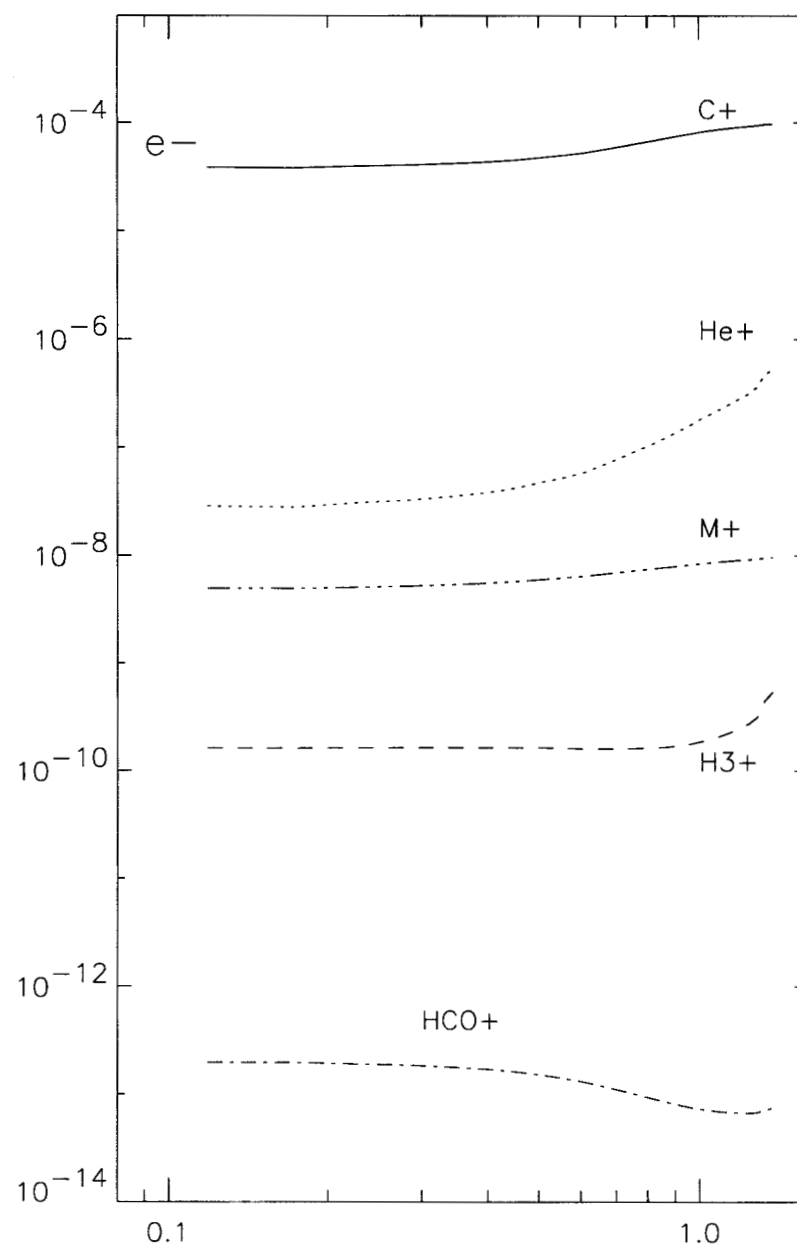
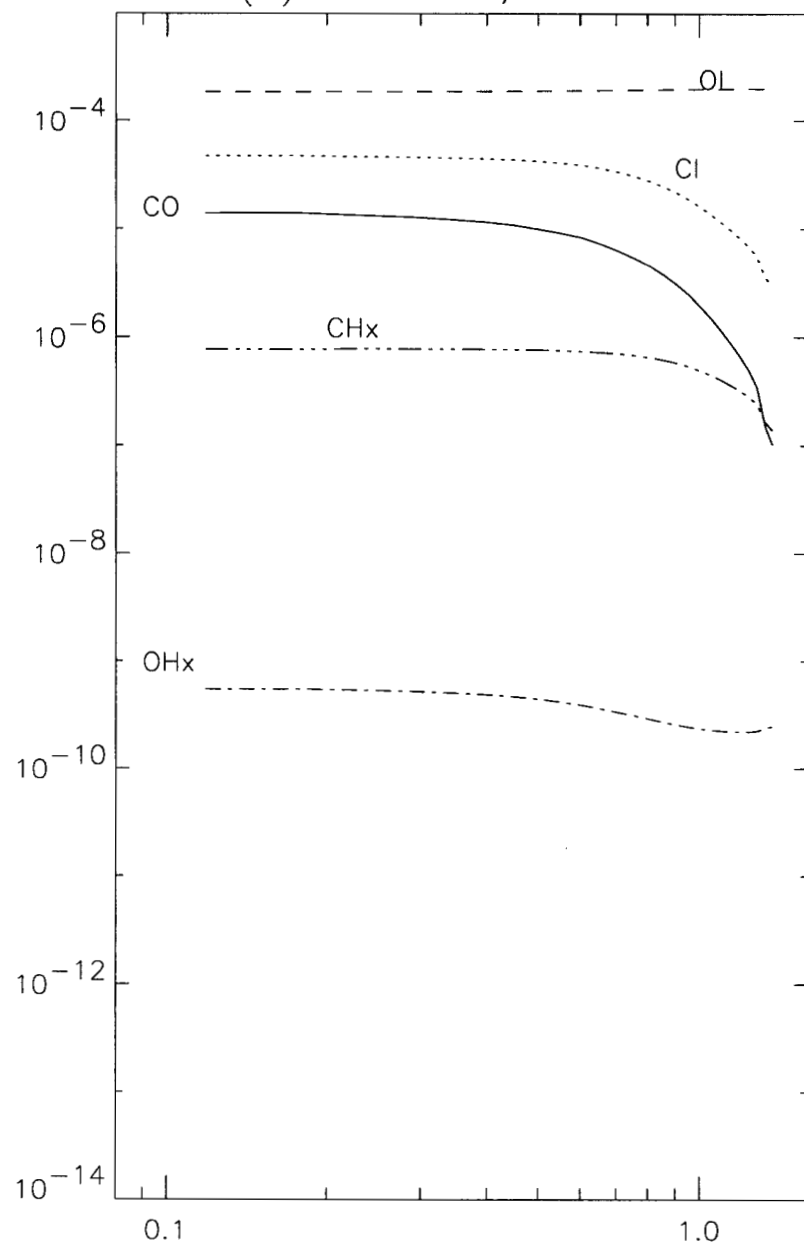
TIME (free fall units) = 6.0115, MODEL 400M3



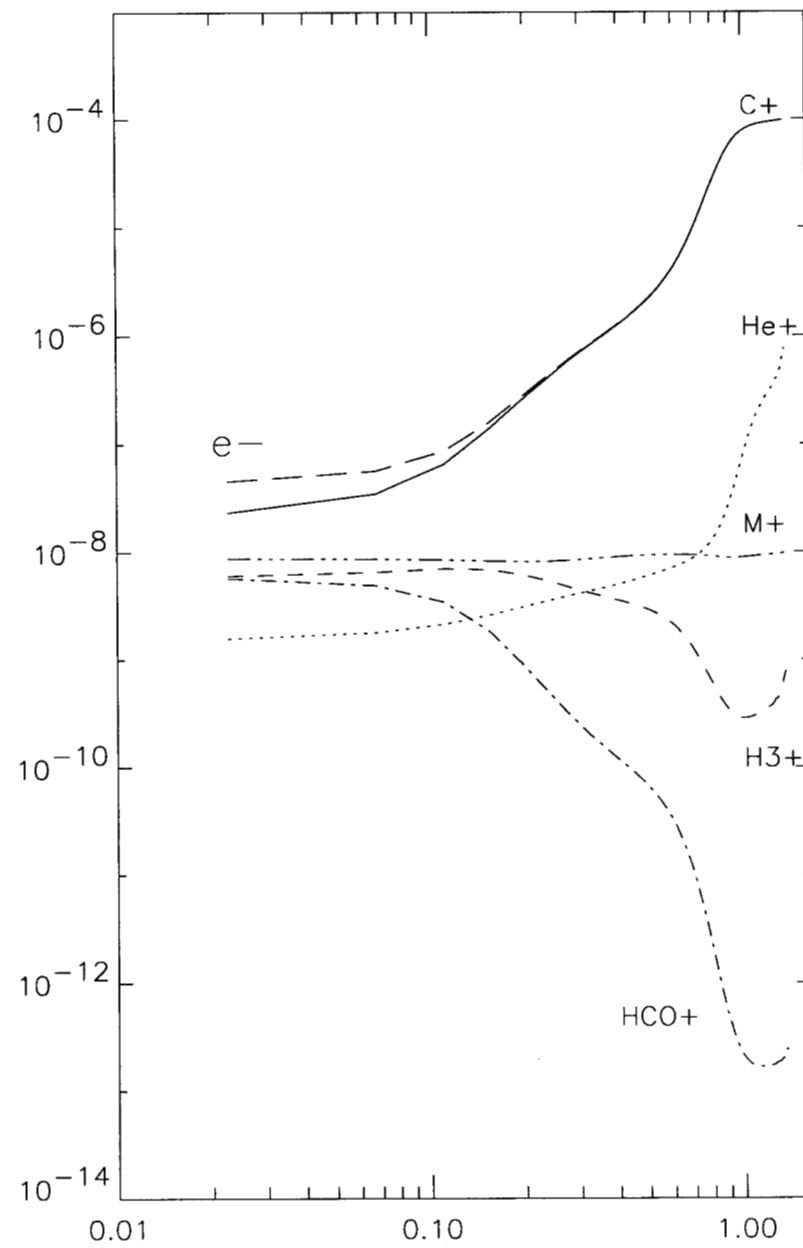
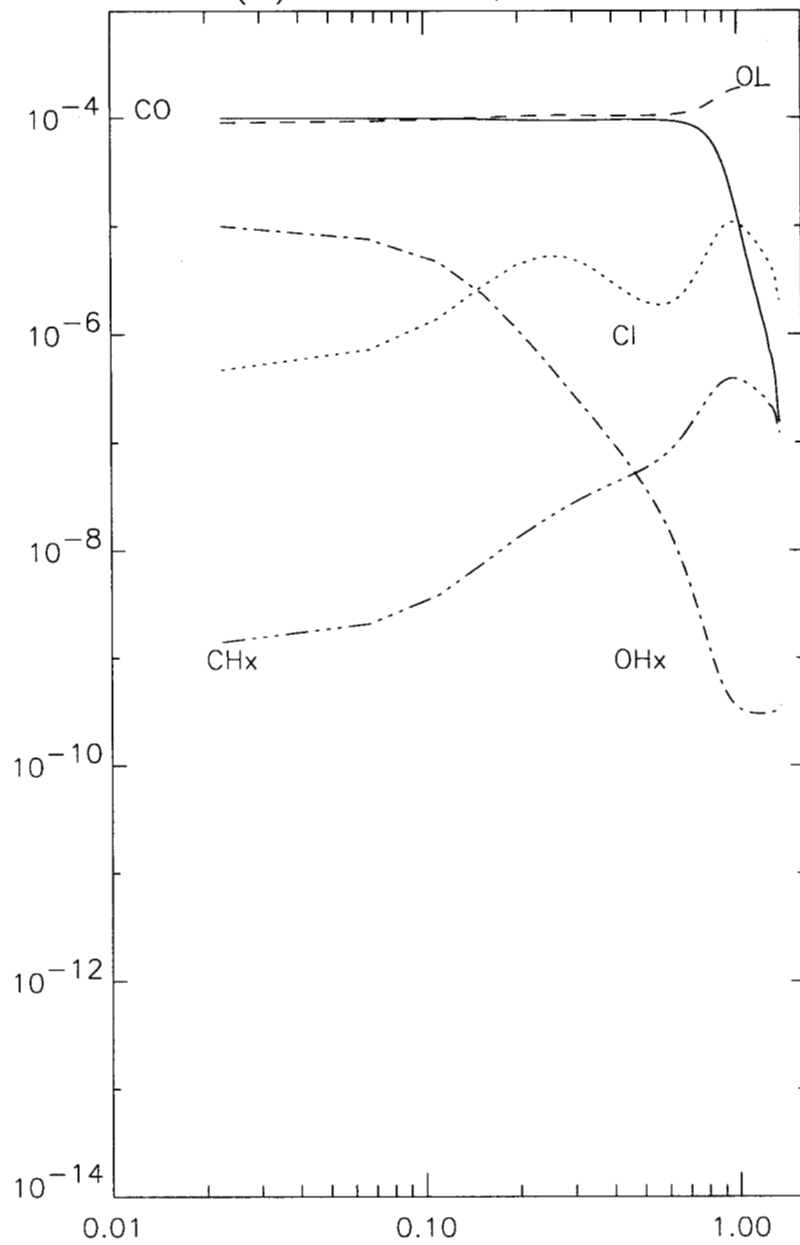
TIME (free fall units) = 6.0802, MODEL 400M3



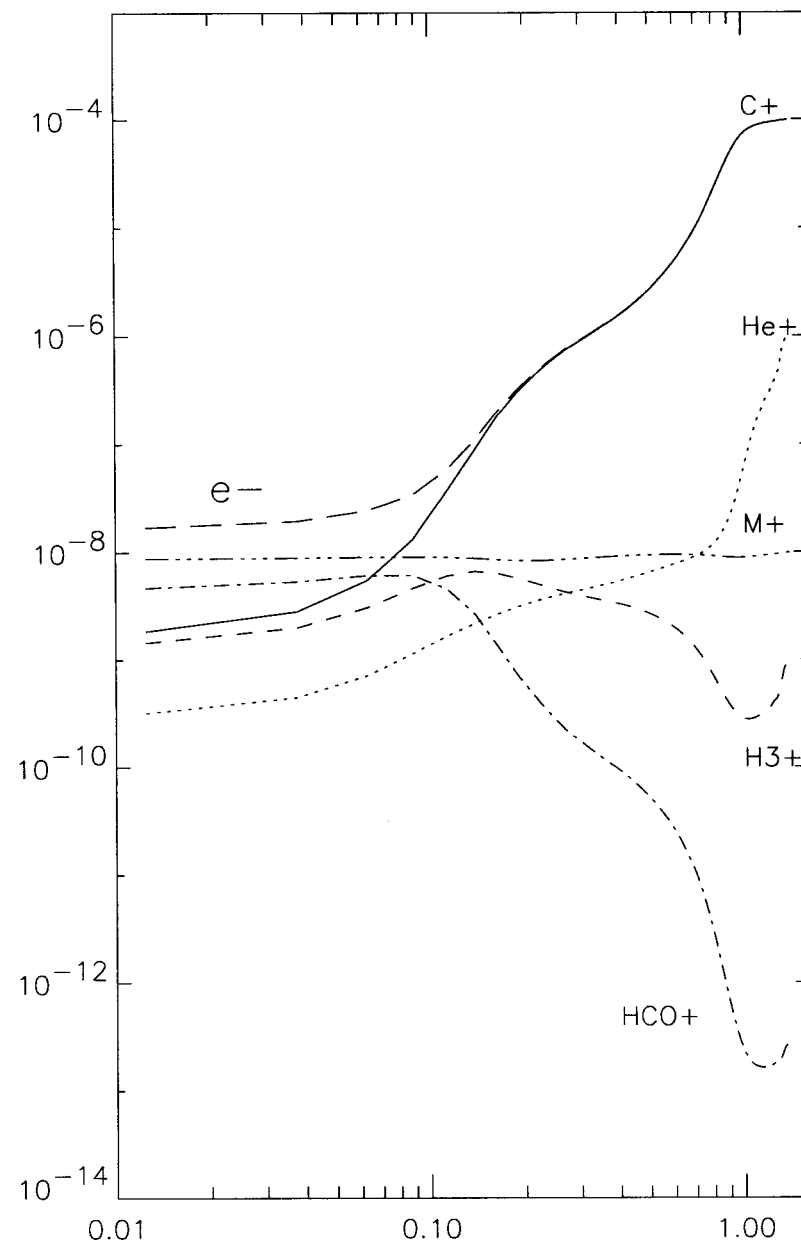
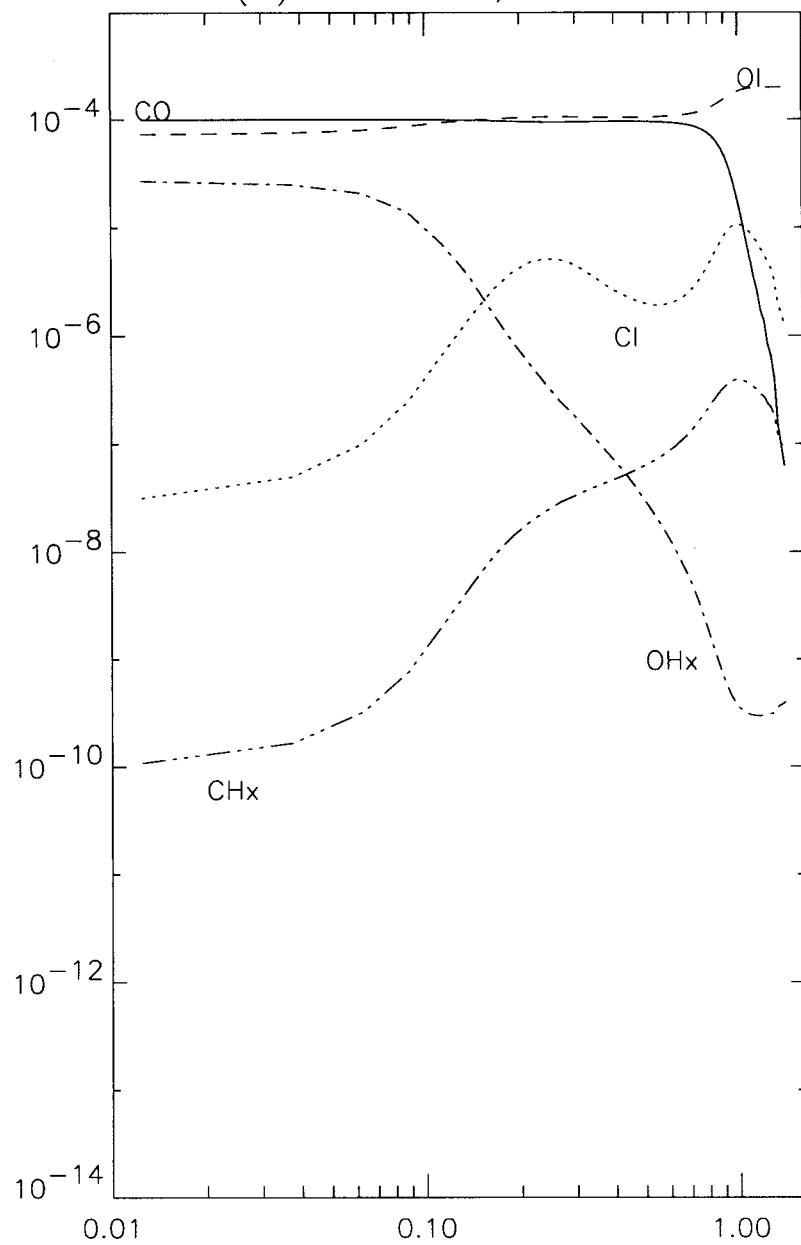
TIME (ff) = 0.0043, MODEL 400M3



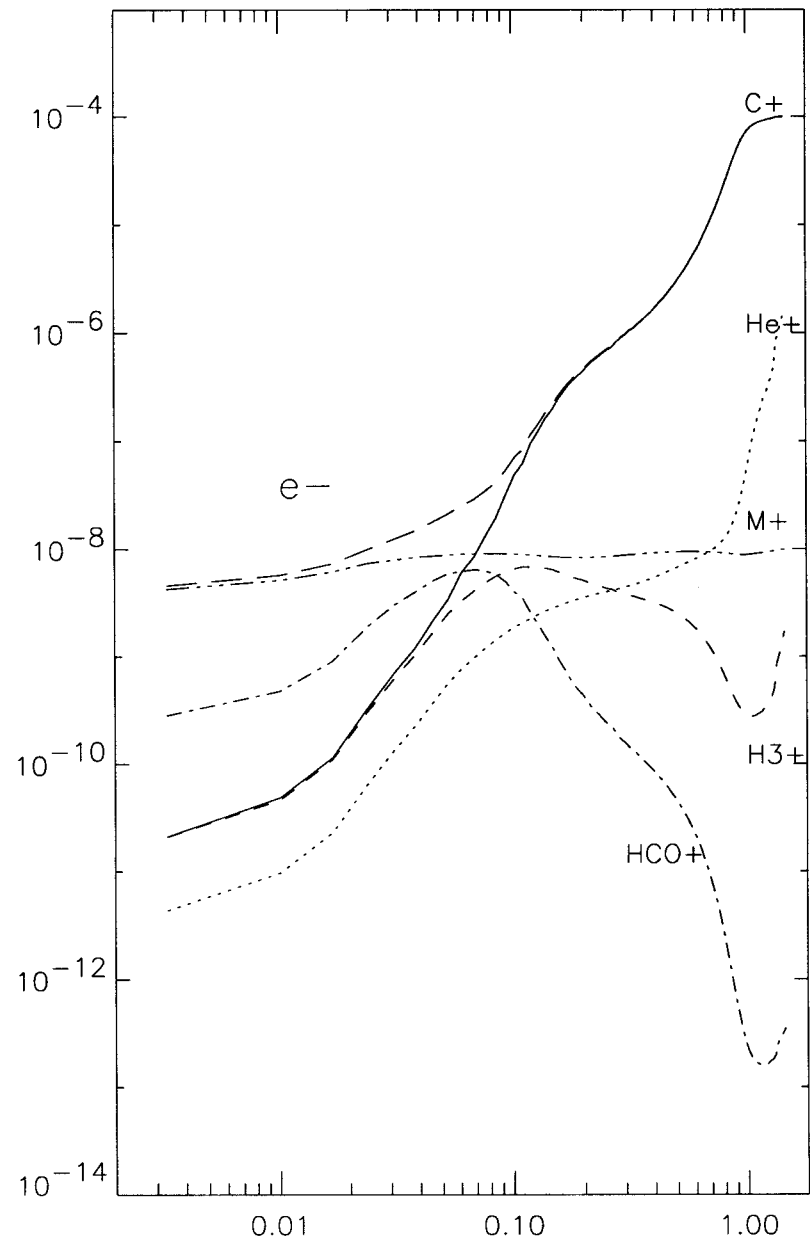
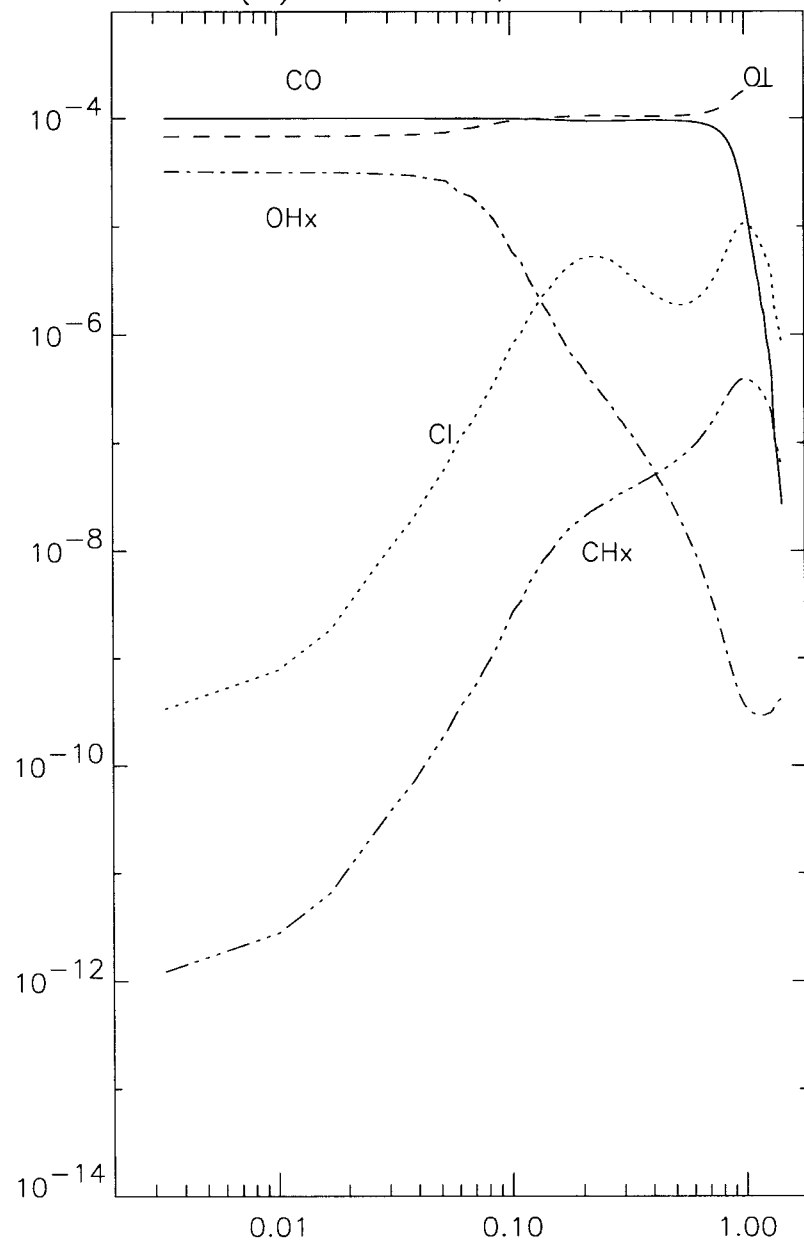
TIME (ff) = 2.2417, MODEL 400M3



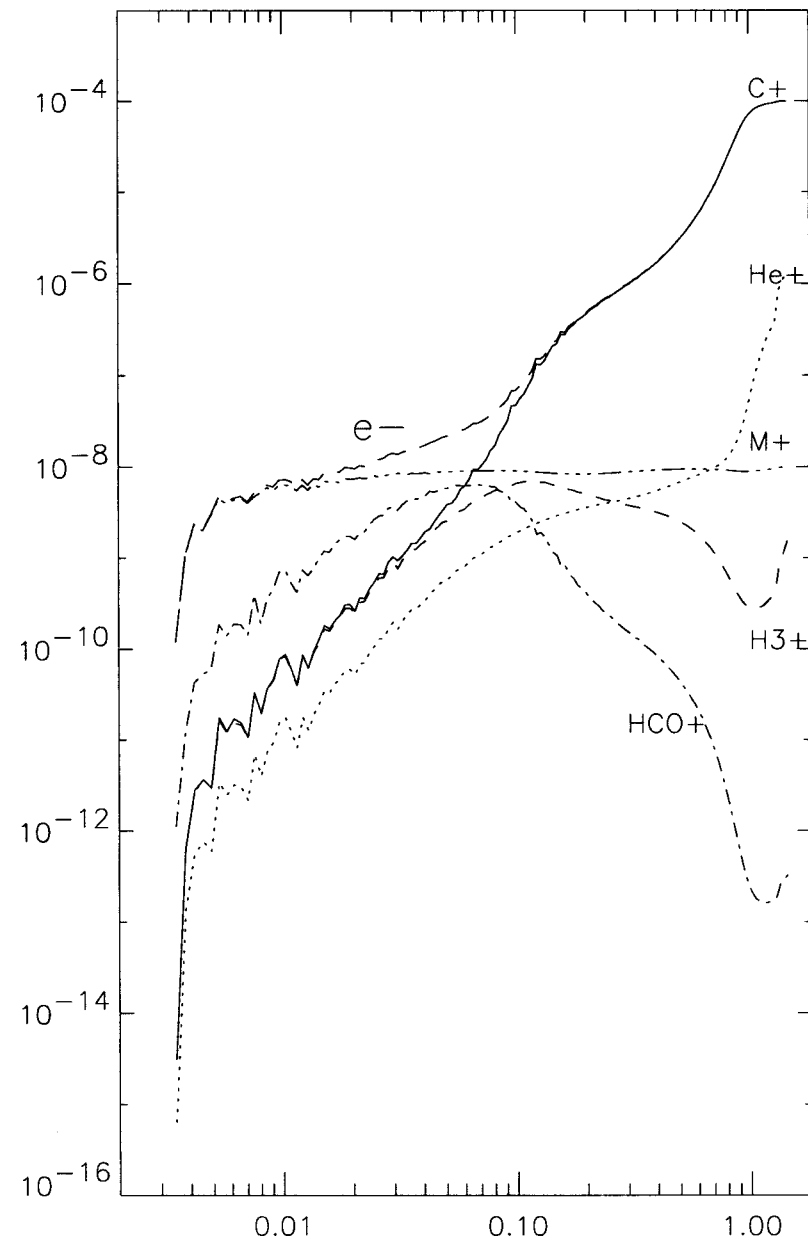
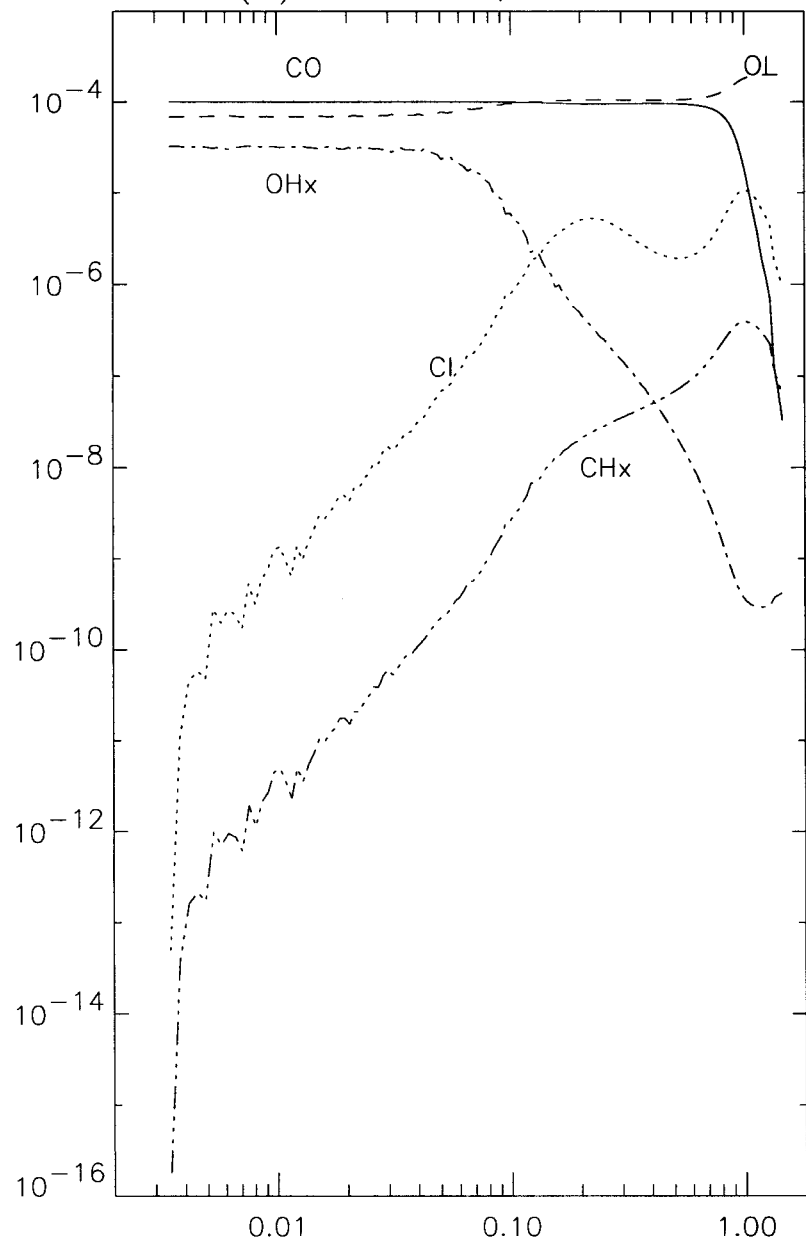
TIME (ff) = 3.8574, MODEL 400M3

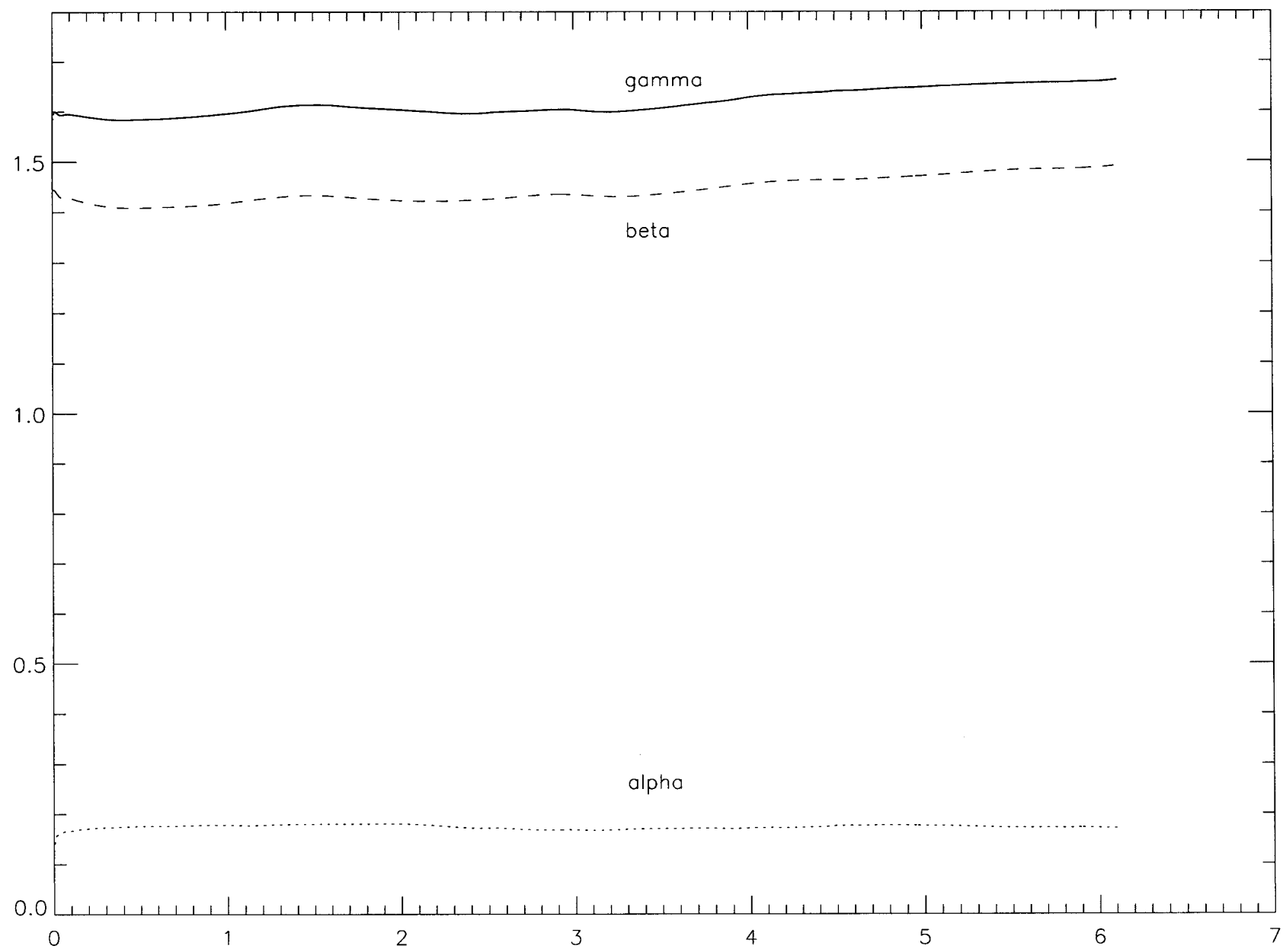


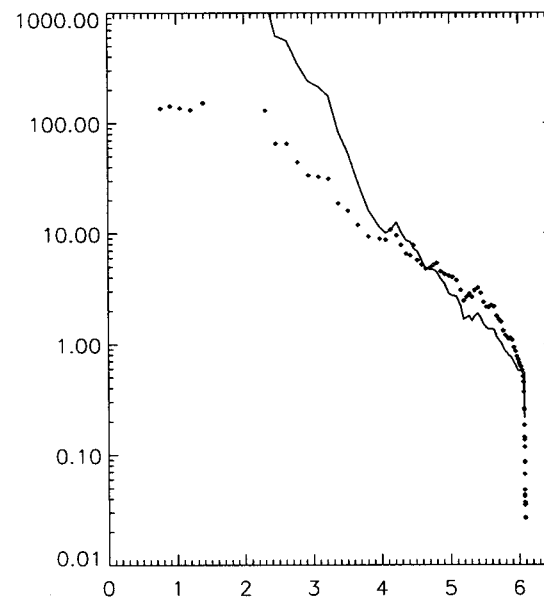
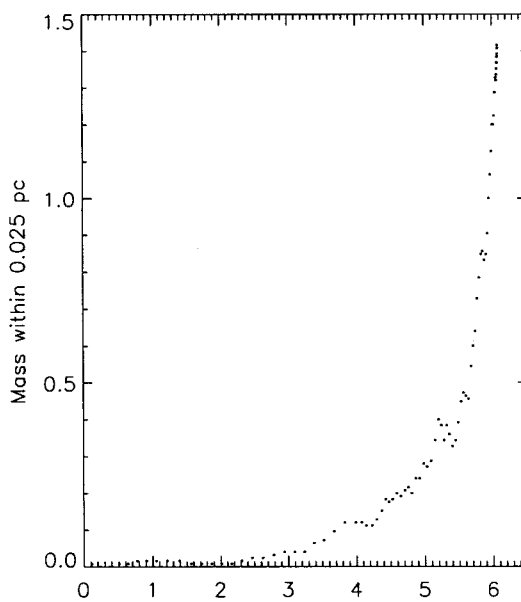
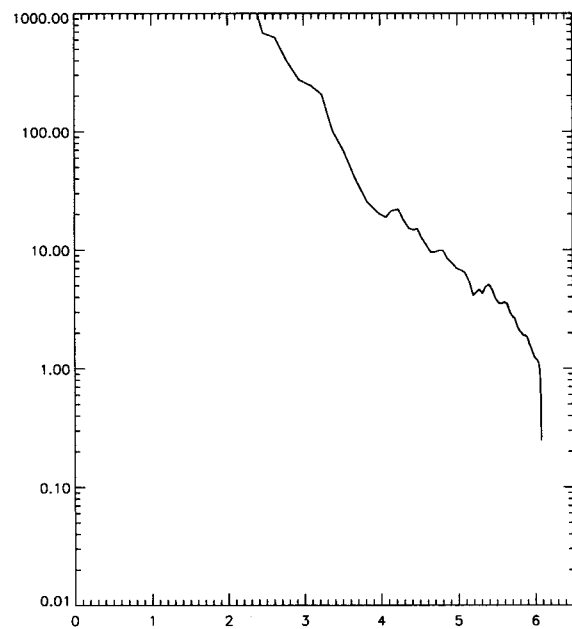
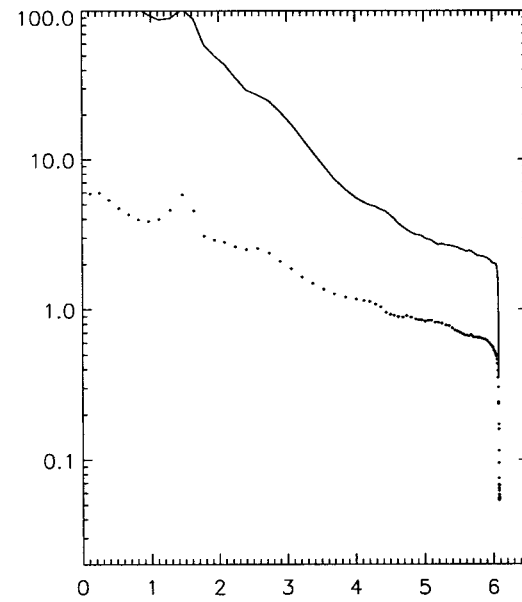
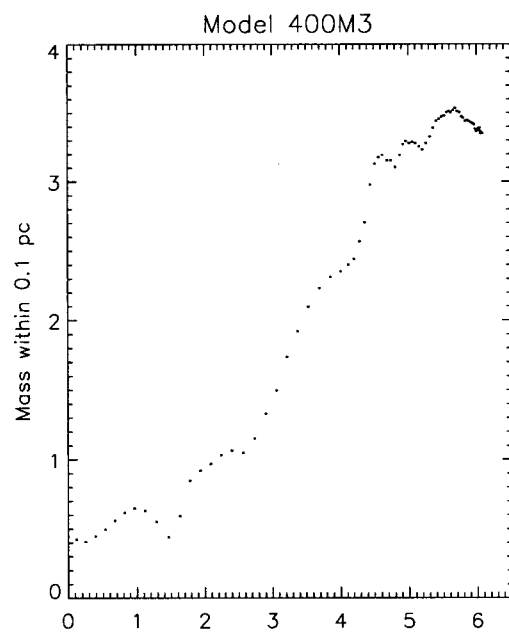
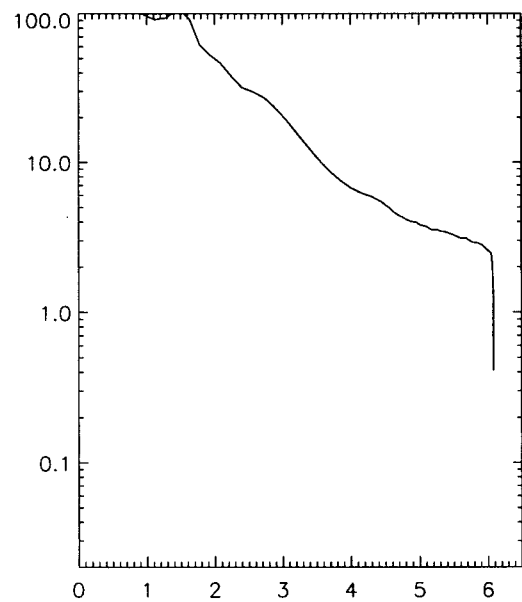
TIME (ff) = 6.0115, MODEL 400M3



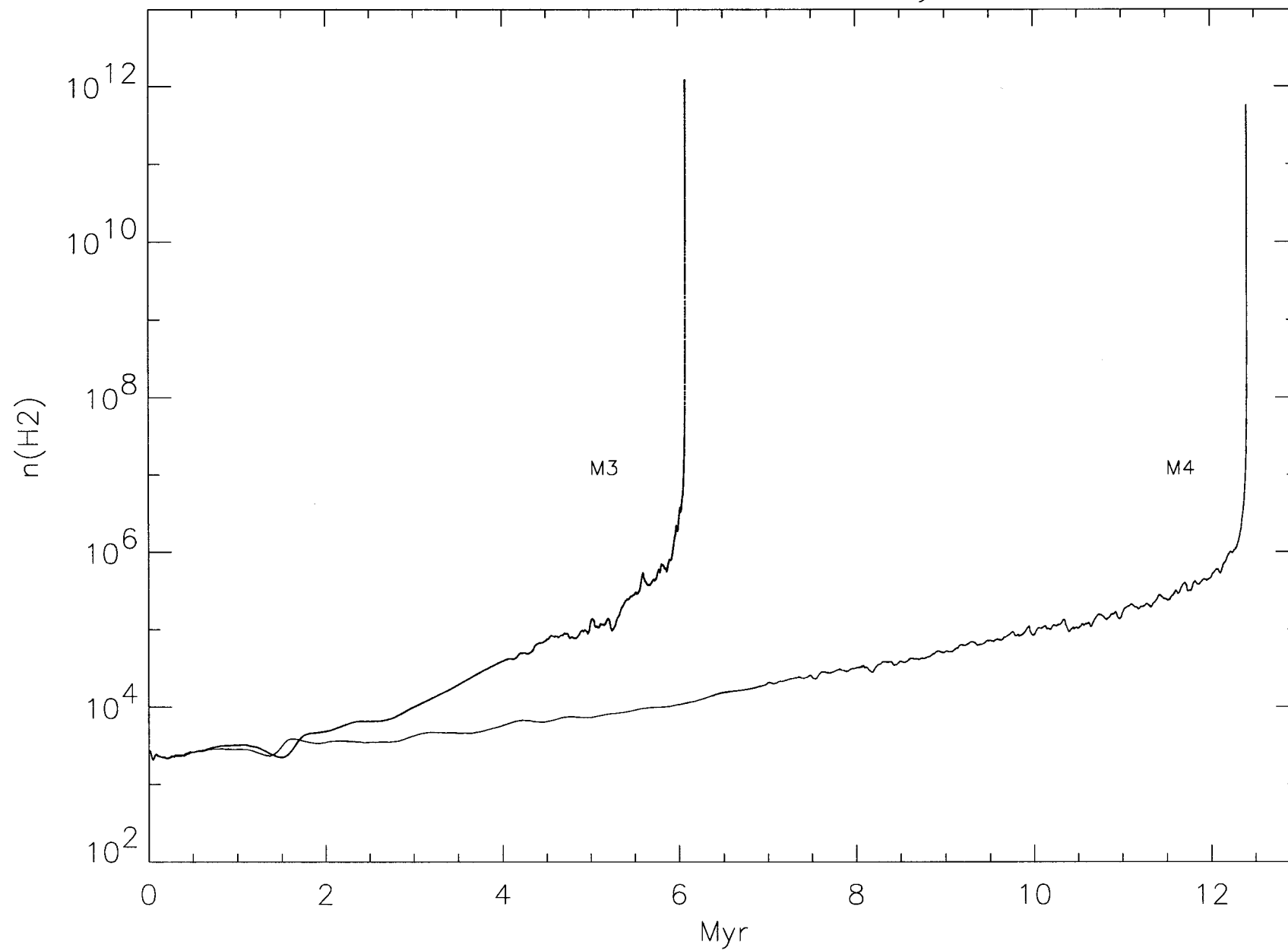
TIME (ff) = 6.0802, MODEL 400M3



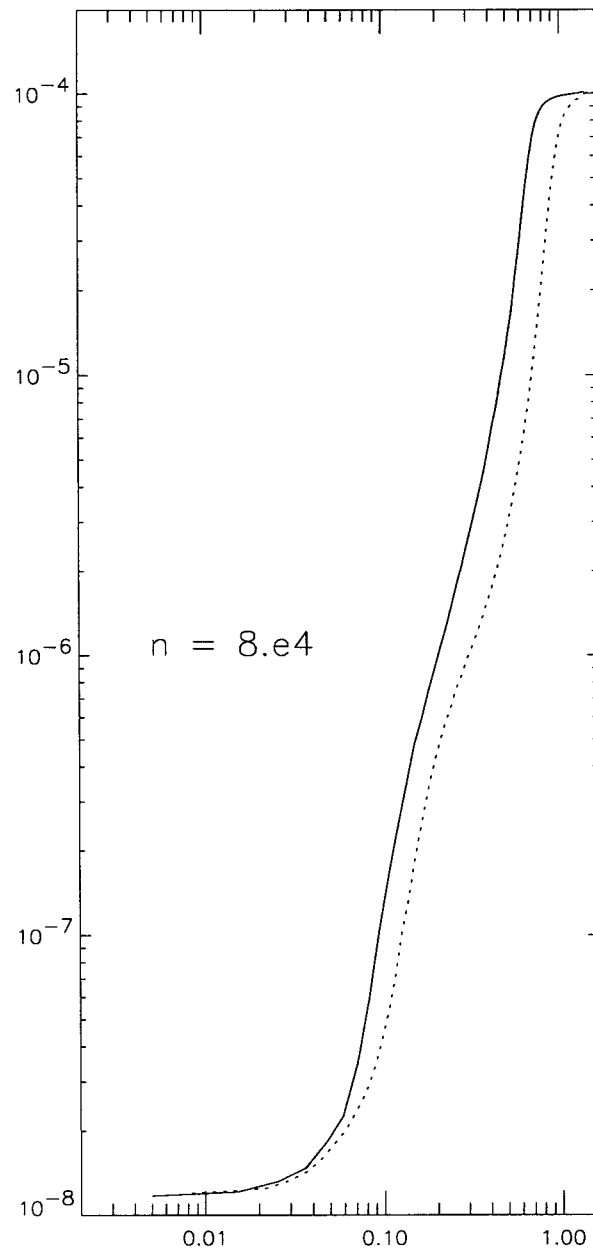
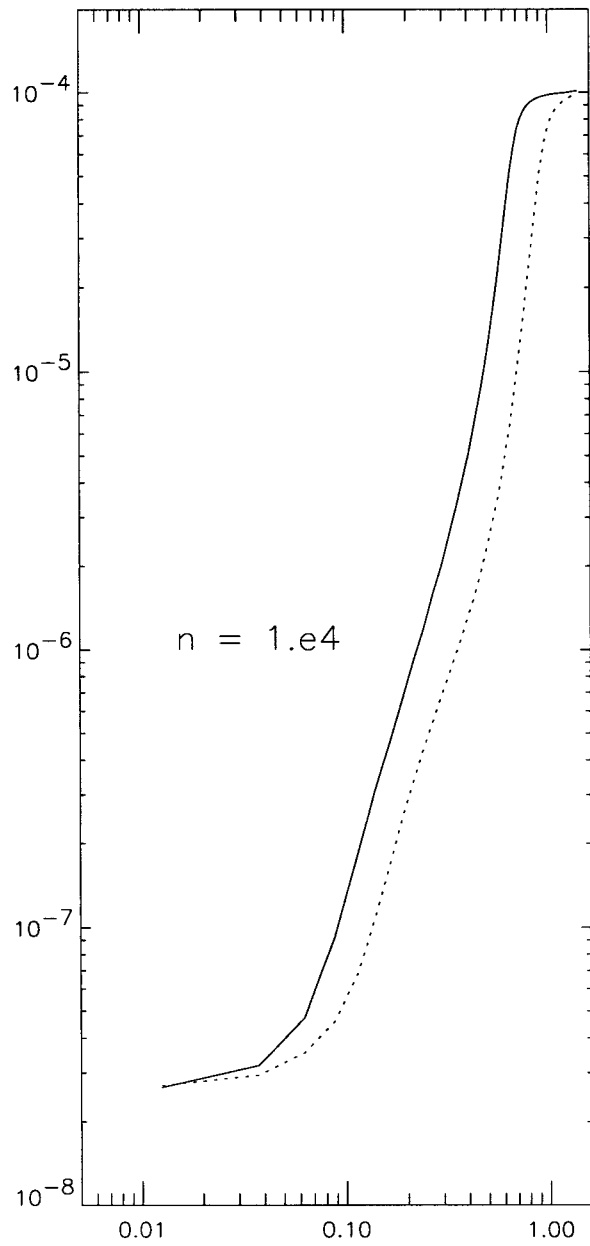
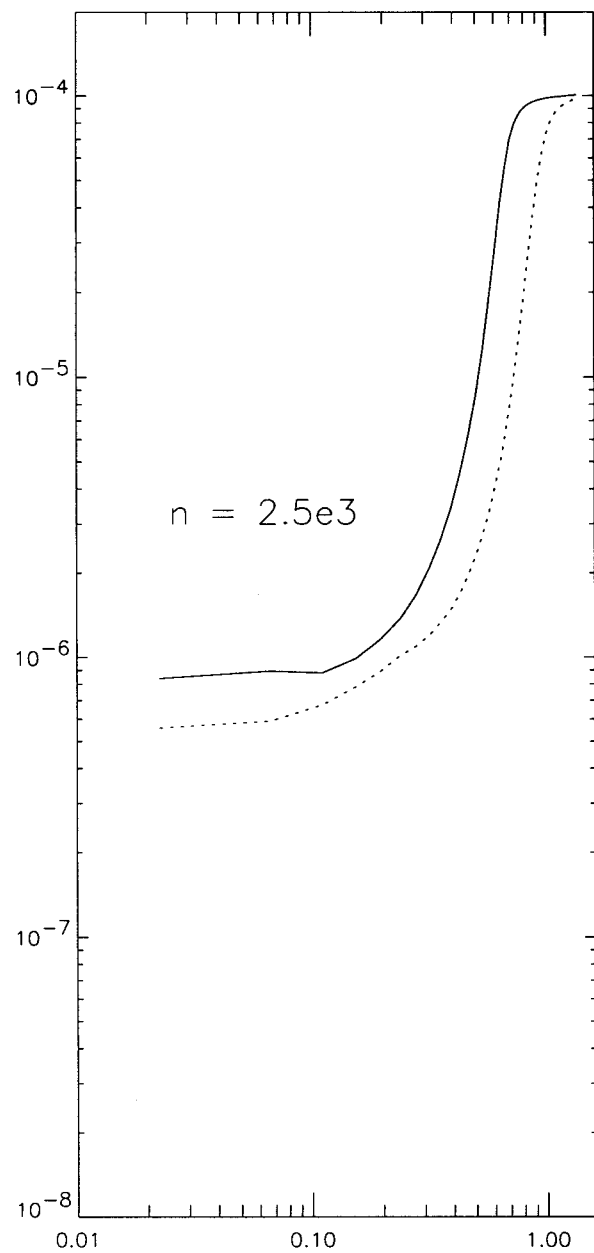




Central number density



ion abundance vs. radius



Central number density

